

Nighttime oxidation of surfactants at the air–water interface

Sebastiani, Federica; Campbell, Richard A.; Rastogi, Kunal ; Pfrang, Christian

DOI:

[10.5194/acp-18-3249-2018](https://doi.org/10.5194/acp-18-3249-2018)

License:

Creative Commons: Attribution (CC BY)

Document Version

Publisher's PDF, also known as Version of record

Citation for published version (Harvard):

Sebastiani, F, Campbell, RA, Rastogi, K & Pfrang, C 2018, 'Nighttime oxidation of surfactants at the air–water interface: effects of chain length, head group and saturation', *Atmos. Chem. Phys*, vol. 18, no. 5, pp. 3249-3268. <https://doi.org/10.5194/acp-18-3249-2018>

[Link to publication on Research at Birmingham portal](#)

Publisher Rights Statement:

Checked for eligibility: 16/08/2018

General rights

Unless a licence is specified above, all rights (including copyright and moral rights) in this document are retained by the authors and/or the copyright holders. The express permission of the copyright holder must be obtained for any use of this material other than for purposes permitted by law.

- Users may freely distribute the URL that is used to identify this publication.
- Users may download and/or print one copy of the publication from the University of Birmingham research portal for the purpose of private study or non-commercial research.
- User may use extracts from the document in line with the concept of 'fair dealing' under the Copyright, Designs and Patents Act 1988 (?)
- Users may not further distribute the material nor use it for the purposes of commercial gain.

Where a licence is displayed above, please note the terms and conditions of the licence govern your use of this document.

When citing, please reference the published version.

Take down policy

While the University of Birmingham exercises care and attention in making items available there are rare occasions when an item has been uploaded in error or has been deemed to be commercially or otherwise sensitive.

If you believe that this is the case for this document, please contact UBIRA@lists.bham.ac.uk providing details and we will remove access to the work immediately and investigate.



Supplement of

Nighttime oxidation of surfactants at the air–water interface: effects of chain length, head group and saturation

Federica Sebastiani et al.

Correspondence to: Christian Pfrang (c.pfrang@reading.ac.uk)

The copyright of individual parts of the supplement might differ from the CC BY 4.0 License.

1. Materials and Preliminary Characterisation

Table 1: List of the organic surfactants used for the experiments including molecular weight (MW) and scattering length (SL). * indicates the custom-deuterated molecules provided by the Oxford Deuteration Facility.

Molecule	Chemical formula	MW / g mol ⁻¹	SL / fm
<i>d</i> ₃₃ MO*	CD ₃ (CD ₂) ₇ CD=CD(CD ₂) ₇ CO ₂ CH ₃	329.69	346.80
<i>d</i> ₃₄ OA	CD ₃ (CD ₂) ₇ CD=CD(CD ₂) ₇ CO ₂ D	316.67	358.05
<i>d</i> ₁₄ POA*	CH ₃ (CH ₂) ₅ CH=CH(CD ₂) ₇ CO ₂ H	268.49	151.49
<i>d</i> ₃₅ SA	CD ₃ (CD ₂) ₁₆ CO ₂ H	319.69	360.98

The thermodynamic properties of the organic monolayers have been investigated by measuring the pressure isotherm as a function of the surface area on a Langmuir trough.¹ The in plane structure of the monolayer was monitored with Brewster angle microscopy (BAM) imaging while compressing the film to record the isotherm. Those two techniques used in combination allowed the characterization of the phase behavior of the single component monolayer, revealing the phase transition regions and the optical properties, such as anisotropy. OA and MO reach a plateau and they form lenses on top of the isotropic monolayer, while POA does not reach a clear plateau and the monolayer remains isotropic all over the compression. The surface pressure reached at the plateau is similar for OA and POA, while MO reaches a much lower pressure. This suggests a lower chain ordering for MO due to the poor hydrophilicity of the head group compared to the parent fatty acid, OA. SA shows in plane structure already at 0 mNm⁻¹ and further compression leads to solid-like structures.

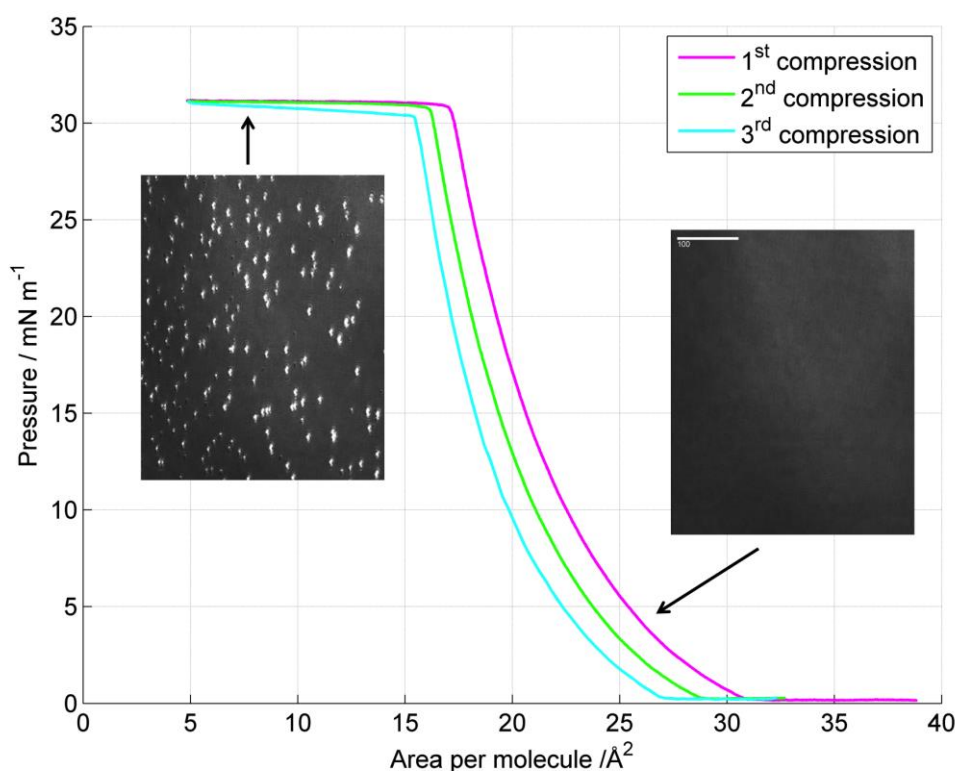


Figure 1. Surface pressure isotherm of *hMO* at 25 °C on a water subphase with the corresponding BAM images of the monolayer recorded at two pressures: 3 mNm⁻¹: the layer is isotropic; and 16.2 mNm⁻¹: the layer is collapsed. The white bar corresponds to 100 μm.

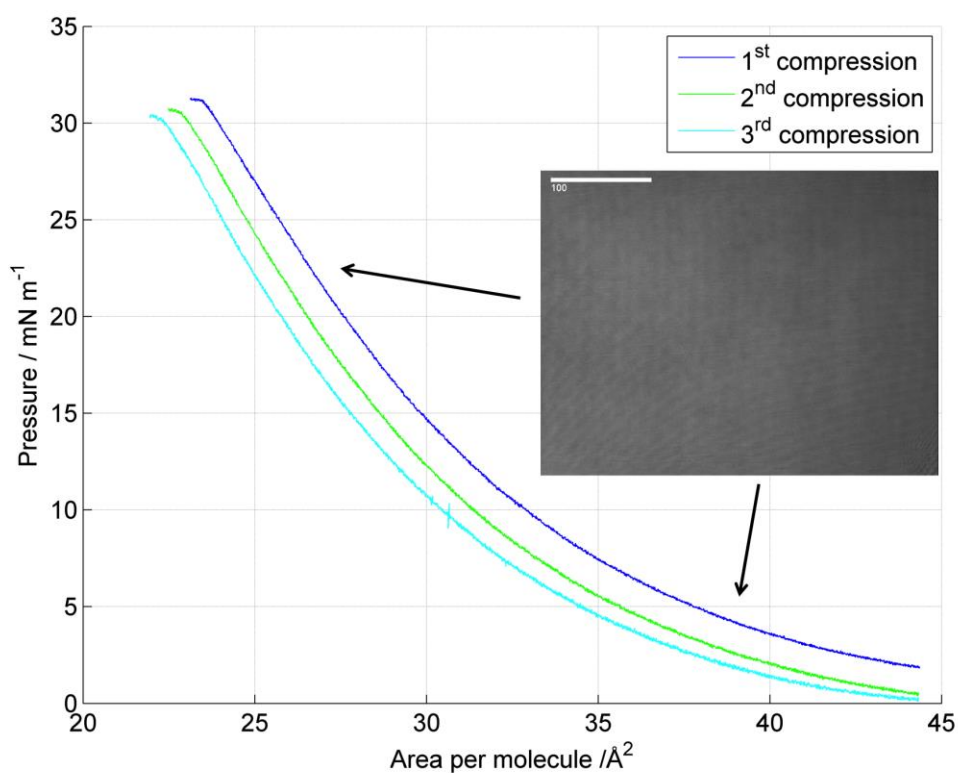


Figure 2. Surface pressure isotherm of *hPOA* at 25 °C on a water subphase with the corresponding BAM image recorded at low pressure. The layer is isotropic at all pressures.

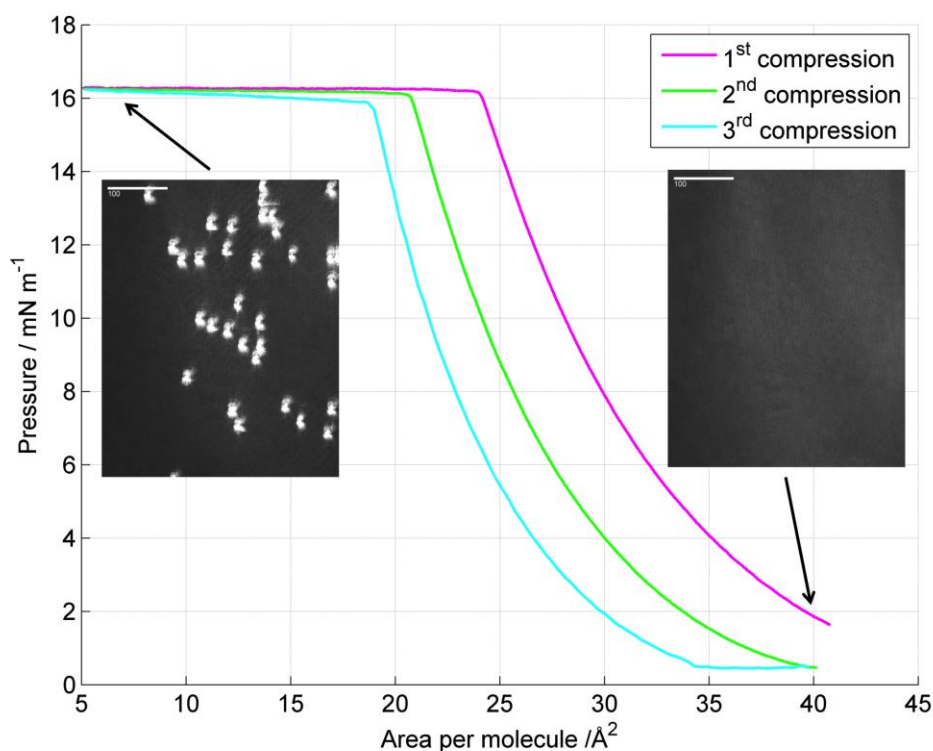


Figure 3. Surface pressure isotherm of *hOA* at 25 °C on a water subphase with the corresponding BAM images recorded at two pressures: 3 mNm⁻¹: the layer is isotropic; and 32 mNm⁻¹: the layer is collapsed. The white bar corresponds to 100 μm.

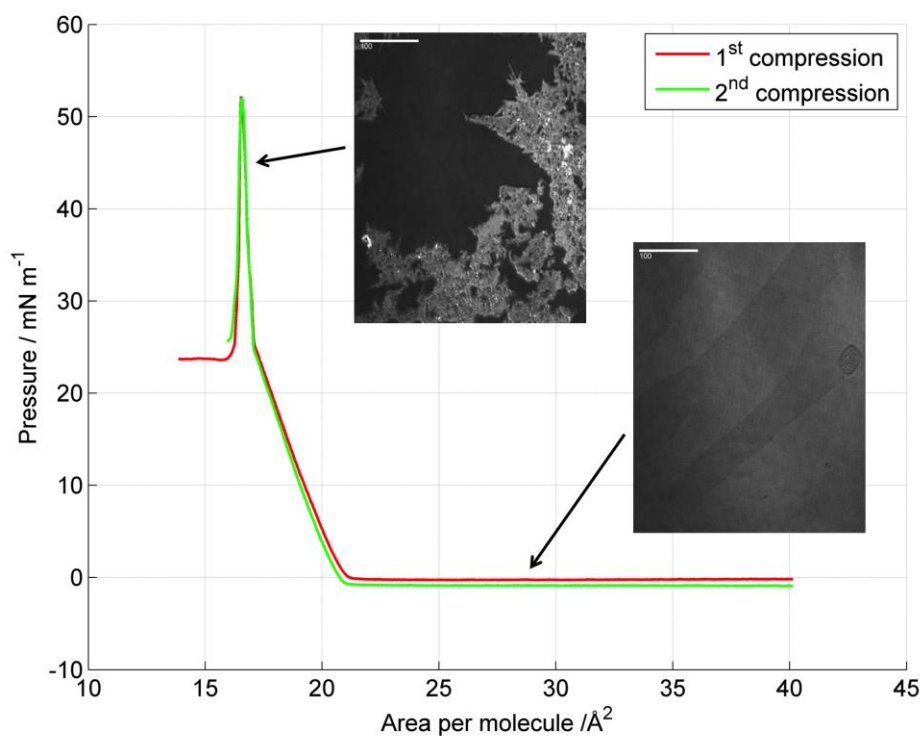


Figure 4. Surface pressure isotherm of *hSA* at 25 °C on a water subphase with corresponding BAM images recorded at two pressures: 0 mNm⁻¹: domains can be distinguished; and 45 mNm⁻¹: organised structures are formed. The white bar corresponds to 100 μm.

2. Gas Flow System

Fig. 5 shows a sketch of the gas flow system. For the production of NO_3 , the O_2 flow was kept at $1.2 \text{ dm}^3 \text{ min}^{-1}$ and the flow rate of NO_2 ranged between 0.06 to $0.36 \text{ dm}^3 \text{ cm}^{-1}$. The mixing bulb has a volume of 5 dm^3 , and the inlet part is made of a glass cylinder with 21 small holes on the surface, which enhances mixing of the components. The residence time in the mixing bulb ranges from 2 to 4 minutes, which is long enough to establish equilibrium within the products. The concentration of NO_3 is tuned by changing the NO_2 flow rate and hence its concentration. $[\text{NO}_2]$ is always in large excess of $[\text{O}_3]$ to ensure that all the ozone is consumed before the gas flow reaches the organic film.

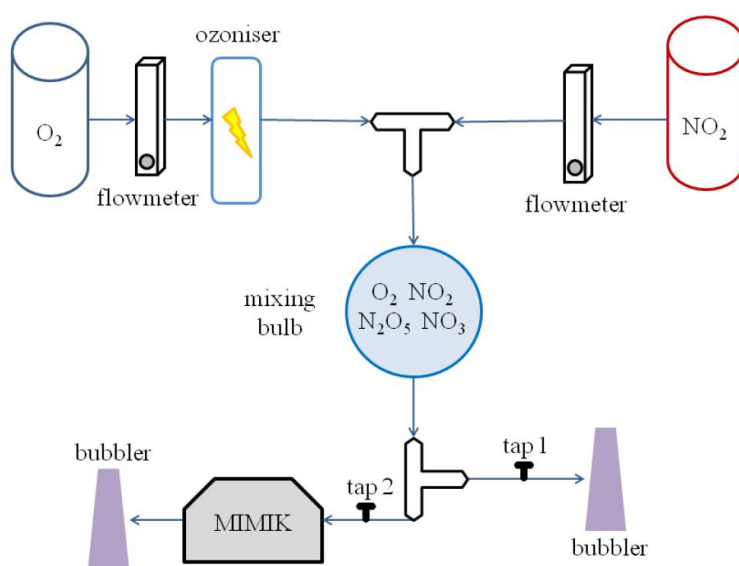


Figure 5. Schematic of the gas flow system. The arrow represents the direction of the flow. On the top left side the ozone is produced, then it mixes with NO_2 just before the inlet of the mixing bulb. From the mixing bulb the mixture can directly go to an exhaust bubbler or pass through the reaction chamber.

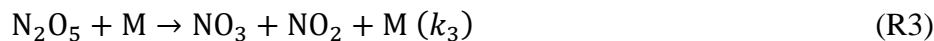
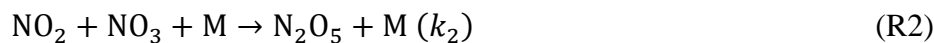
The tubing is made from Chemfluor[®] (PTFE), with an outer diameter of 1/4 inch and an inner diameter of 1/8 inch; this material has been chosen for its high chemical resistance. A digital flow meter (Model MV-302, MASS-VIEW, Bronkhorst) has been used for the control of the O_2 flow. For the NO_2 a ball flow meter (Cole Parmer) resistant to NO_2 corrosion has been used. All the connectors used were made of Teflon or stainless steel to ensure chemical resistance.

3. Reaction Model and Spectroscopic Measurements

We produced NO₃ by reacting varying concentrations of NO₂ with a given ozone concentration. [NO₃] could not be measured directly, but we calculated [NO₃] from spectroscopic measurements of [NO₂] and [N₂O₅].

3.1 Reaction model

The reactions considered for description of the *in situ* production of NO₃ are shown below:



In order to simulate the reactions, the concentrations of the gas-phase species are calculated as a function of time relying on published rate coefficients evaluated in the review "Chemical kinetics and photochemical data for use in atmospheric studies (evaluation No. 17)" by Sander *et al.*² (the type of reaction and the ambient conditions, *i.e.* temperature and pressure are appropriately taken into account; the conditions chosen for the calculation are 298.15 K (25 °C) and atmospheric pressure, 1 atm). For further details on the following Eqs 1–7 see Seinfeld and Pandis, 2006.³ The first reaction is a bimolecular reaction and the rate coefficient is described as:

$$k_1(T) = Ae^{-(E/RT)} \quad (1)$$

$A = 1.2 \times 10^{-13} \text{ cm}^3 \text{ molecule}^{-1} \text{ s}^{-1}$ and $E/R = 2450 \text{ K}$,² those values are valid for temperature ranging from 230 to 360 K. Reaction R2 is a termolecular reaction and the rate coefficient, $k_2(T, [M])$, is estimated using the expression described by Troe⁴. The concentration of the third body, [M], is related directly to the pressure, in the atmosphere M is the sum of N₂ and O₂ and approximating to ideal gas we can use $[M] = N_{\text{Av}}/V_{\text{mole}} = 2.46 \times 10^{19} \text{ molecule cm}^{-3}$.

$$k_2(T, [M]) = \frac{k_{0,2}(T)[M]}{1 + (k_{0,2}(T)[M]/k_{\infty,2}(T))} 0.6 \left[1 + (\log(k_{0,2}(T)[M]/k_{\infty,2}(T)))^2 \right]^{-1} \quad (2)$$

where $k_{0,2}(T)$ is the low-pressure limiting value for $k_2(T, [M])$ and the dependence on temperature is expressed as:^{3,4}

$$k_{0,2}(T) = k_{0,2}^{300} \left(\frac{T}{300} \right)^{-n} \quad (3)$$

where $k_{0,2}^{300} = 2 \times 10^{-30} \text{ cm}^6 \text{ molecule}^{-2} \text{ s}^{-1}$ is the value at 300 K and $n = 4.4$ (valid for T in the range 200 – 300 K), both values were taken from Ref.². The $k_{\infty,2}(T)$ is the high-pressure limit value for $k_2(T,[M])$ and the dependence on temperature is expressed as:^{3,4}

$$k_{\infty,2}(T) = k_{\infty,2}^{300} \left(\frac{T}{300} \right)^{-m} \quad (4)$$

where $k_{\infty,2}^{300} = 1.4 \times 10^{-12} \text{ cm}^3 \text{ molecule}^{-1} \text{ s}^{-1}$ is the value at 300 K and $m = 0.7$ (valid for temperature in the range 200 – 400 K), both values were taken from Sander *et al.*²

Reaction R3 is similar to the previous one,⁴ but the calculation of $k_{0,3}$ and $k_{\infty,3}$ is slightly different, see Eqs 6 and 7.

$$k_3(T, [M]) = \frac{k_{0,3}(T)[M]}{1 + (k_{0,3}(T)[M]/k_{\infty,3}(T))} 0.6 \left[1 + (\log(k_{0,3}(T)[M]/k_{\infty,3}(T)))^2 \right]^{-1} \quad (5)$$

The low-pressure limit for $k_3(T,[M])$ is calculated as:

$$k_{0,3}(T) = k_{0,3}^{300} \left(\frac{T}{300} \right)^{-p} e^{-L/T} \quad (6)$$

where $k_{0,3}^{300} = 1.3 \times 10^{-3} \text{ cm}^3 \text{ molecule}^{-1} \text{ s}^{-1}$ is the value at 300 K, $L = 11000 \text{ K}$ and $p = 3.5$ (valid for temperature ranging from 200 to 400 K), all values stated were taken from Sander *et al.*² The high-pressure limit for $k_3(T,[M])$ is expressed as:

$$k_{\infty,3}(T) = k_{\infty,3}^{300} \left(\frac{T}{300} \right)^q e^{-N/T} \quad (7)$$

where $k_{\infty,3}^{300} = 9.7 \times 10^{14} \text{ cm}^3 \text{ molecule}^{-1} \text{ s}^{-1}$ is the value at 300 K, $N = 11080 \text{ K}$ and $q = 0.1$ (valid for temperature in the range 200 – 400 K). All the values are taken from Sander *et al.*²

Table 2. Estimation of the rate constants for the reactions R1 – R3 in the conditions: $T = 25^\circ\text{C}$ and pressure 1 atm.

Rate	Value
$k_1(298.15 \text{ K})$	$3.2 \times 10^{-17} \text{ cm}^3 \text{ molecule}^{-1} \text{ s}^{-1}$
$k_2(298.15 \text{ K})$	$1.18 \times 10^{-12} \text{ cm}^3 \text{ molecule}^{-1} \text{ s}^{-1}$
$k_3(298.15 \text{ K})$	0.06 s^{-1}

Once all the rate coefficients are obtained for the correct conditions (Table 2), the differential equations describing the reactions R1 – R3 (Eqs 8 – 11) can be solved numerically in order to obtain the concentrations as a function of time for the various chemical compounds.

$$\frac{d[\text{O}_3]}{dt} = -k_1[\text{O}_3][\text{NO}_2] \quad (8)$$

$$\frac{d[\text{NO}_2]}{dt} = -k_1[\text{O}_3][\text{NO}_2] - k_2[\text{NO}_2][\text{NO}_3] + k_3[\text{N}_2\text{O}_5] \quad (9)$$

$$\frac{d[\text{N}_2\text{O}_5]}{dt} = k_2[\text{NO}_2][\text{NO}_3] - k_3[\text{N}_2\text{O}_5] \quad (10)$$

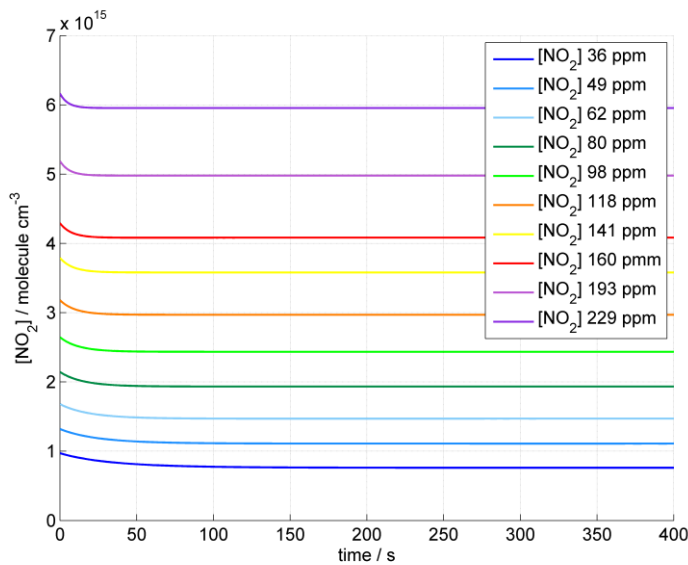
$$\frac{d[\text{NO}_3]}{dt} = k_1[\text{O}_3][\text{NO}_2] - k_2[\text{NO}_2][\text{NO}_3] + k_3[\text{N}_2\text{O}_5] \quad (11)$$

4

5 The system of equations has been implemented in Matlab.⁵ The solutions have been
 6 computed for several initial $[\text{NO}_2]$ values, corresponding to the gas conditions chosen for the
 7 NR and IR experiments. The initial concentration of ozone was fixed to 1.05×10^{14} molecule
 8 cm^{-3} . This value was obtained from the calibration of the ozoniser performed with the UV-
 9 Vis using a flow rate of $1.2 \text{ dm}^3 \text{ min}^{-1}$.

10 Figs 6–9 show the concentrations of the various gas species as a function of time and their
 11 dependence on the initial NO_2 concentrations.

12



13

14 **Figure 6.** Time evolution of $[\text{NO}_2]$ calculated from Eqs 8–11 for several initial values of
 15 $[\text{NO}_2]$. The initial values of $[\text{NO}_2]$ are reported in the legend.

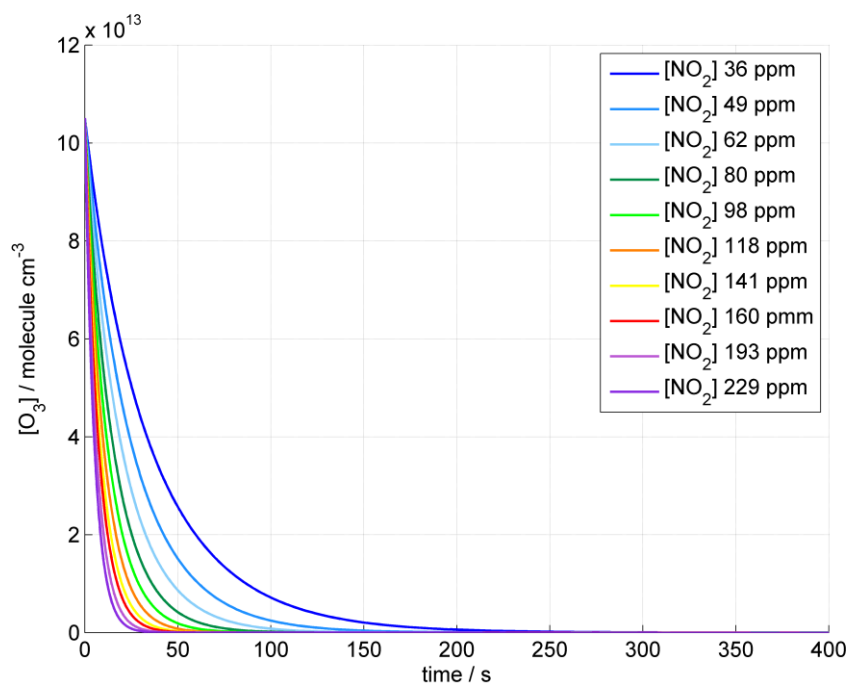


Figure 7. The consumption of O_3 as a function of t , calculated from Eqs 8–11 as a function of different initial $[\text{NO}_2]$ values is displayed.

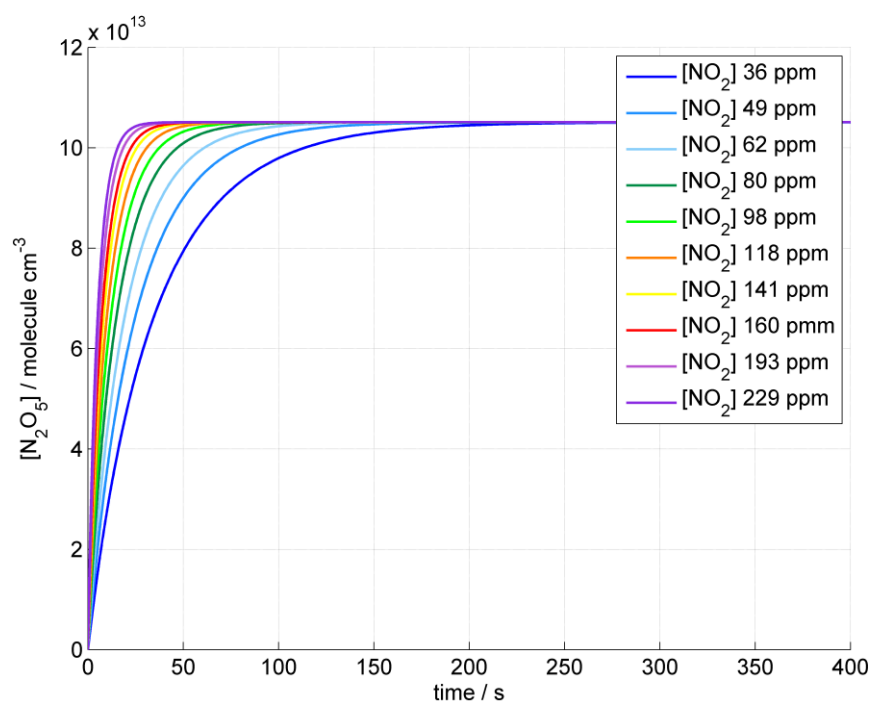


Figure 8. The formation of $[\text{N}_2\text{O}_5]$ as a function of t , calculated from Eqs 8–11 for several initial values of $[\text{NO}_2]$ is shown.

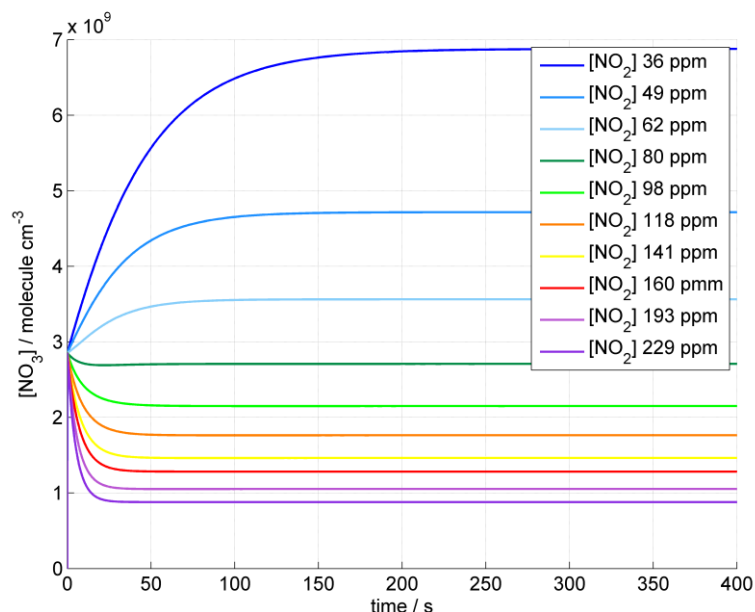


Figure 9. The formation of $[\text{NO}_3]$ as a function of t , calculated from Eqs 8–11 for several initial values of $[\text{NO}_2]$ is shown.

Since the concentrations reach constant values quickly, the data are reported just for $t \leq 400$ s. NO_2 reaches the steady state concentration faster when the initial $[\text{NO}_2]$ is higher. Ozone is totally consumed in less than 250 s (see Fig. 7). The concentration of NO_3 produced ranges from 36 ppt to 279 ppt, and it is lower when the excess of NO_2 is higher (see Fig. 9). The steady state concentrations of N_2O_5 are always approaching the same value (Fig. 8) that is determined by the initial ozone concentration.

In the experimental gas-setup a 5 dm^3 mixing bulb was used to allow the reaching of steady-state concentrations of the gas species before they entered the reaction chamber. In the NR measurements conducted at the Institut Laue-Langevin (Grenoble, France), the reaction chamber was situated in a temperature-controlled sample area while the mixing bulb was situated simply in the guide hall where the temperature was not well controlled.

An additional study of the gas system focused on the temperature dependence of the steady state concentrations to establish the impact of warm weather during the NR measurements. The rate constants (k_1 , k_2 and k_3) were estimated for several temperature values and used for solving the differential Eqs 8–11. The purpose was to estimate specifically the time needed to reach a new steady state concentration due to the change in temperature between the mixing bulb in the guide hall and the reaction chamber in the sample area. For example, to calculate the steady state concentrations at $T = 30^\circ\text{C}$ the values calculated at $T = 25^\circ\text{C}$ were used as initial conditions for the differential equations and the solutions were computed. Fig. 10 show

the evolution of concentrations due to temperature increase (initial $[\text{NO}_2] = 36 \text{ ppm}$). It is apparent that only a few tens of milliseconds are enough to reach the new constant concentrations. (Note that the computed values for O_3 are meaningless since they are virtually zero; $\approx 10^{-31} \text{ molecule cm}^{-3}$.) Evidence of this rapid establishment of equilibrium conditions following a temperature change is essential information in the interpretation of the experimental data recorded with NR.

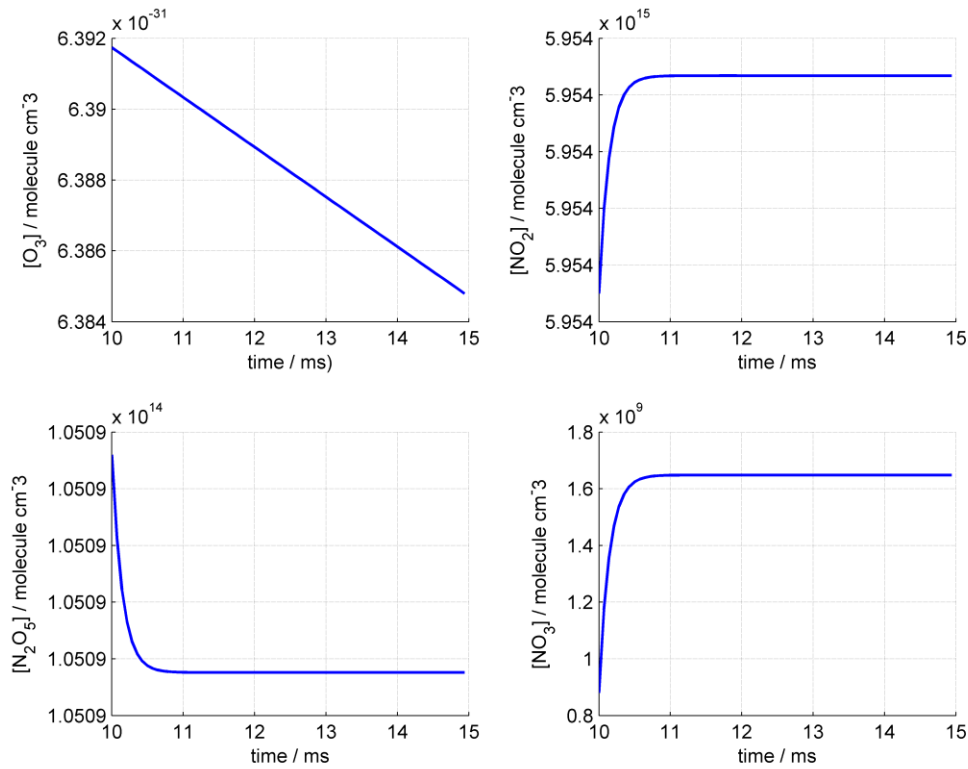


Figure 10. The evolution of the concentrations of O_3 , NO_2 , N_2O_5 and NO_3 due to temperature increase from 25°C to 30°C (the initial concentration of NO_2 is 36 ppm). The equilibrium is reached in tens of milliseconds. (please note that the computed values for O_3 are meaningless since they are virtually zero).

The development of this model provides the means to calculate the NO_3 concentration from the concentrations of NO_2 and N_2O_5 . Those concentrations may be measured by IR spectroscopy. Once the reactions R1 – R3 achieve the steady states the measured values for $[\text{NO}_2]$ and $[\text{N}_2\text{O}_5]$ allow calculation of the $[\text{NO}_3]$ using the following equation:

$$\frac{d[\text{NO}_3]}{dt} = 0 \Rightarrow [\text{NO}_3] = \frac{k_1[\text{O}_3][\text{NO}_2] + k_3[\text{N}_2\text{O}_5]}{k_2[\text{NO}_2]} \quad (12)$$

$$t \geq 400 \text{ s}, [\text{O}_3] \rightarrow 0, [\text{NO}_3] \cong \frac{k_3[\text{N}_2\text{O}_5]}{k_2[\text{NO}_2]} \quad (13)$$

3.2 IR measurements

The measurements of the concentrations have been performed with an FTIR spectrometer (IFS/66 S, Bruker). For the very low concentrations to be detected, the most sensitive detector of the FTIR spectrometer was chosen which was a photoconductive detector (MCT D315). The acquired spectrum was averaged over 100 scans and the resolution was fixed to 1 cm^{-1} . A systematic study of the gas mixture composition as a function of $[\text{NO}_2]$ was performed. $[\text{NO}_2]$ in the cylinder was 1000 ppm in air, to obtain various concentrations the flow rate of NO_2 was varied from $45\text{ cm}^3\text{ min}^{-1}$ to $360\text{ cm}^3\text{ min}^{-1}$ and mixed with the carrier gas (oxygen) flowing at $1.2\text{ dm}^3\text{ min}^{-1}$ (the resulting concentrations are reported in Table 3).

Table 3. The flow rates of NO_2 are reported in the first column. The resulting concentrations due to mixing with O_2 flowing at $1.2\text{ dm}^3\text{ min}^{-1}$ are reported in the second column.

NO_2 flow rate / $\text{cm}^3\text{ min}^{-1}$	$[\text{NO}_2]$ / ppm
45	36
62	49
80	62
104	80
130	98
161	118
197	141
228	160
290	193
360	229

The O_3 concentration was kept constant at $1.05 \times 10^{14}\text{ molecule cm}^{-3}$ by setting the oxygen flow to $1.2\text{ dm}^3\text{ min}^{-1}$ and the ozoniser exposure to 10 intervals, i.e. maximum UV exposure. Two types of measurements were recorded. First, in order to calculate the absorption cross section for NO_2 , the mixture of O_2 and NO_2 was measured without O_3 production for each flow rate. Secondly, the spectra of the mixture produced by the reactions R1 – R3 were measured in order to record the NO_2 loss and the N_2O_5 production. For each NO_2 flow condition, at least two independent experiments were performed, in order to account for errors due to not ideal reproducibility of the experimental procedures, e.g. flow meter settings. The gas sampling chamber was a glass cylinder with a path length of 18 cm, and two circular CaF_2 windows of a diameter of 2.5 cm. The chamber inlet was connected to the exit of the 5 dm^3 mixing bulb. The outlet was connected to a bubbler. For the connections Teflon tubing and either Teflon or stainless steel gas connectors were used. The flow was admitted to the

1 chamber for 10 minutes, then the chamber taps were closed and the chamber was
2 disconnected from the gas flow system. Immediately after, the chamber was placed in the
3 sample area of the spectrometer and the measurements were recorded. Once the NO₂-O₂
4 mixture was measured, the glass chamber was connected again to the gas flow system and the
5 O₂ was exposed to UV light, after 10 min, the glass chamber filled with the mixture NO₂-O₂-
6 N₂O₅ was again put into the IR measurement area and the data were acquired. Background
7 measurements were recorded with the chamber filled with pure oxygen.

8 The spectral contribution of the atmospheric gases, H₂O and CO₂, was eliminated with the
9 atmospheric compensation routine of the FTIR instrument software. The treatment of the data
10 has been performed with the software provided with the instrument (OPUS 5.5, Bruker). In
11 order to obtain the absorbance due to the investigated gas species the absorbance spectrum
12 recorded for pure oxygen was subtracted from the spectra of the mixture, then a baseline
13 correction was performed fitting a polynomial function to the spectrum excluding the peaks.
14 Examples of absorbance spectra is reported in Fig. 11. The spectra recorded for NO₂-O₂ are
15 compared to the spectra of NO₂-O₂-N₂O₅ with the same initial [NO₂]. The characteristic peaks
16 of NO₂ used in this study were centred at $\approx 1600\text{ cm}^{-1}$ and $\approx 1628\text{ cm}^{-1}$.⁶ A clear decrease of
17 absorbance accounts for the NO₂ consumption due to the reactions R1 – R2. The appearance
18 of three peaks in the spectra of NO₂-O₂-N₂O₅ can be attributed to N₂O₅ and HNO₃. The
19 characteristic peaks used for N₂O₅ are near 1250 cm^{-1} and 1700 cm^{-1} .⁷ HNO₃ absorbs close to
20 1320 cm^{-1} and 1710 cm^{-1} .^{8,9} Initially, we did not expect to measure HNO₃, since the gas flow
21 system was considered to be in dry conditions. The spectra show clearly the presence of
22 HNO₃, which can be attributed to the reaction between N₂O₅ and water. For this reason, the
23 peak at 1700 cm^{-1} has not been used to quantify N₂O₅, because it overlapped with the peak
24 due to nitric acid. The absorbance intensity at 1250 cm^{-1} was used to obtain [N₂O₅] with an
25 absorption cross section of $1.81 \times 10^{-18}\text{ cm}^2\text{ molecule}^{-1}$.⁷

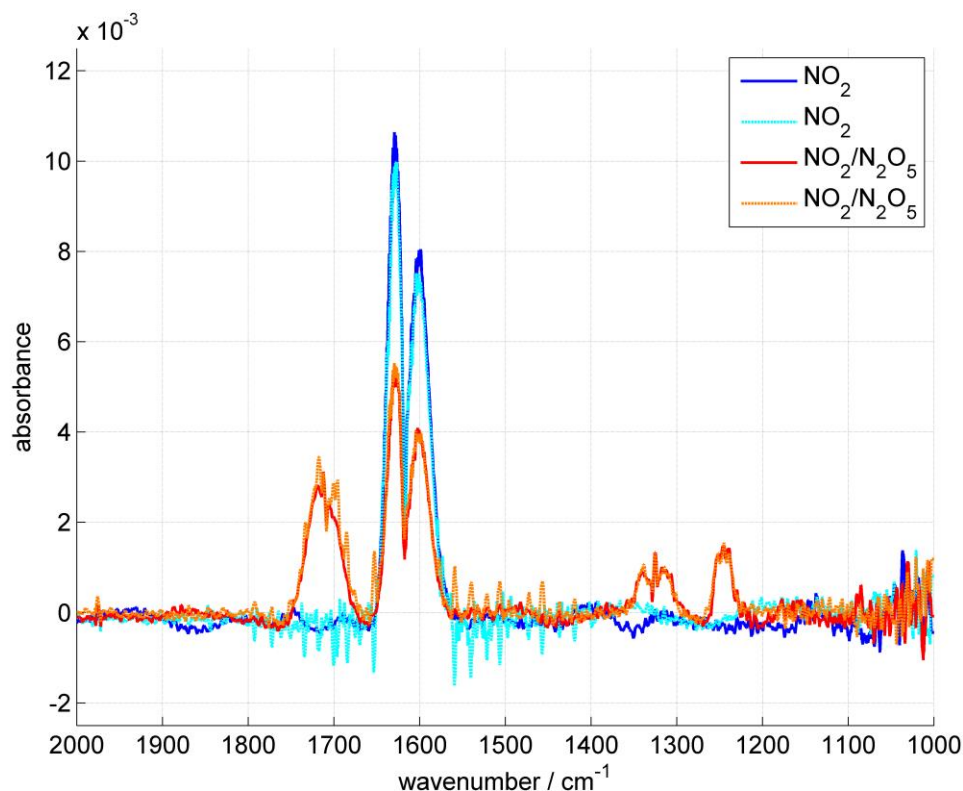


Figure 11. Absorbance spectra recorded with FTIR spectroscopy. The concentration of NO_2 was 36 ppm. The blue solid line and the light blue dashed line represents the spectra recorded for NO_2 carried by O_2 . The red solid line and the orange dashed line refer to the spectra recorded for the mixture of $\text{NO}_2 - \text{N}_2\text{O}_5$ produced by the reactions R1 – R3 and carried by O_2 . The background and baseline subtractions have been performed using the OPUS software.

As found with the theoretical calculation, the concentration of N_2O_5 is not varying as a function of the NO_2 initial concentration. The value obtained is about half of what the model predicted. Since the ozone production is fairly stable and reproducible, we suggest that this reduced N_2O_5 can be explained by the heterogeneous reaction of N_2O_5 with water, which is rapid compared to the gas-phase reaction³ and we found clear spectroscopic evidence of the presence of HNO_3 .

In order to calculate the NO_3 concentration, $[\text{NO}_2]$ is needed. To the best of our knowledge, the absorption cross section for NO_2 , ϵ_{NO_2} , in the IR region is not available, hence we decided to measure this coefficient using the mixture $\text{NO}_2\text{-O}_2$ and then use ϵ_{NO_2} to quantify the concentration of NO_2 after reaction. The actual concentration was derived taking into account the nominal concentration of the NO_2 cylinder (1000 ppm) and the NO_2 flow rate. Figures 12 and 13 show the absorbance peak intensities, with and without O_3 reaction, as a function of the initial NO_2 concentration.

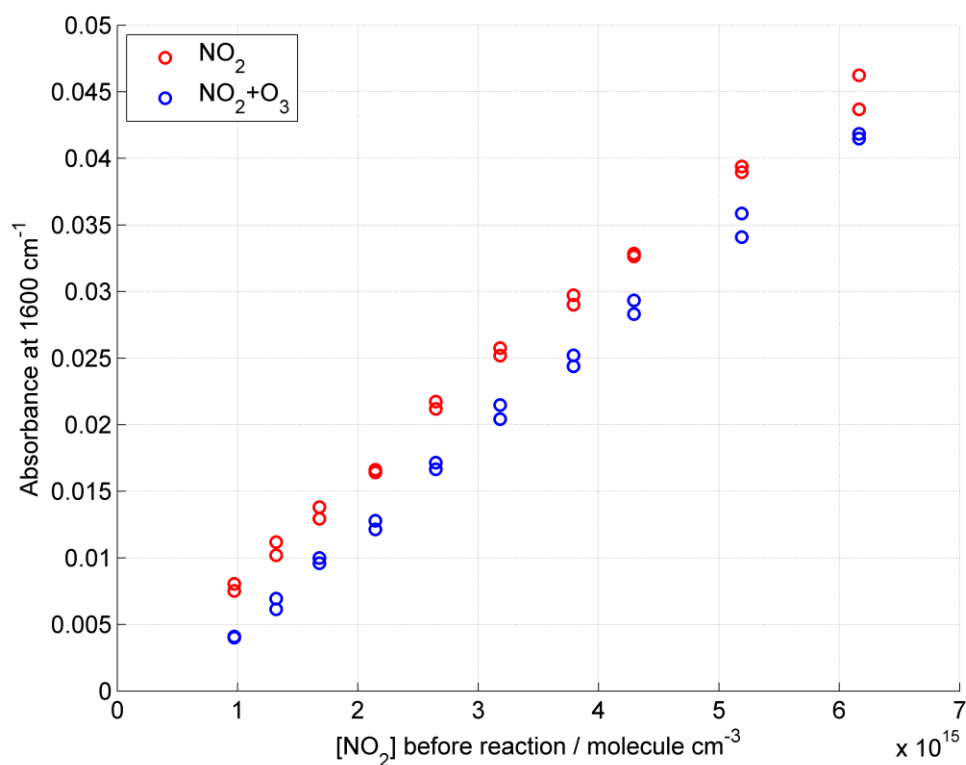


Figure 12. Intensity of the absorbance peak around 1600 cm^{-1} as a function of the initial $[\text{NO}_2]$. Blue circles represent NO_2 mixed with O_3 , red circles represent the NO_2 not exposed to O_3 .

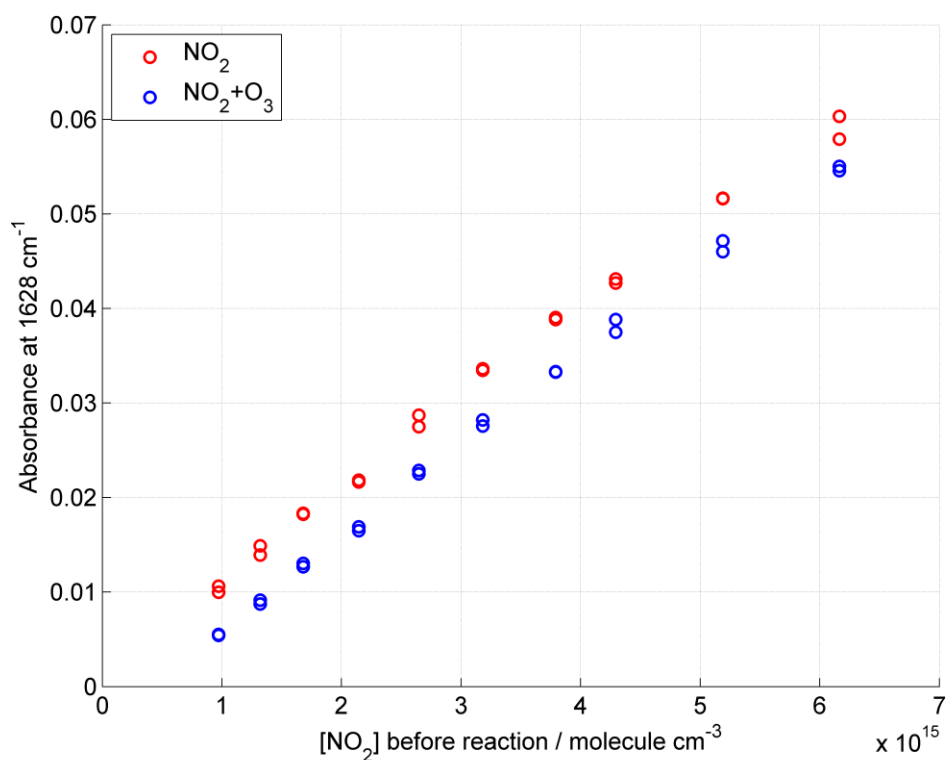


Figure 13. Intensity of the absorbance peak around 1628 cm^{-1} as a function of the initial $[\text{NO}_2]$. Blue circles represent NO_2 mixed with O_3 , red circles represent the NO_2 not exposed to O_3 .

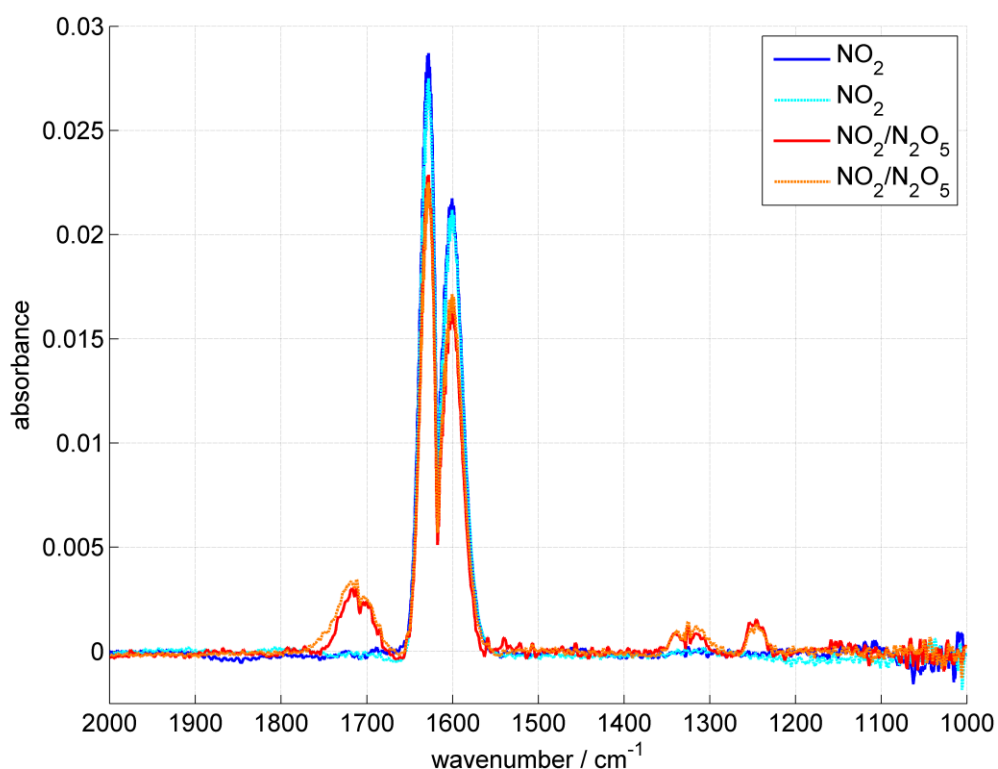


Figure 14. Absorbance spectra recorded with FTIR spectroscopy. The concentration of NO_2 was 98 ppm. The blue solid line and the light blue dashed line represents the spectra recorded for NO_2 carried by O_2 . The red solid line and the orange dashed line refer to the spectra recorded for the mixture of $\text{NO}_2 - \text{N}_2\text{O}_5$ produced by the reactions R1 – R3 and carried by O_2 . The background and baseline subtractions have been performed using the OPUS software.

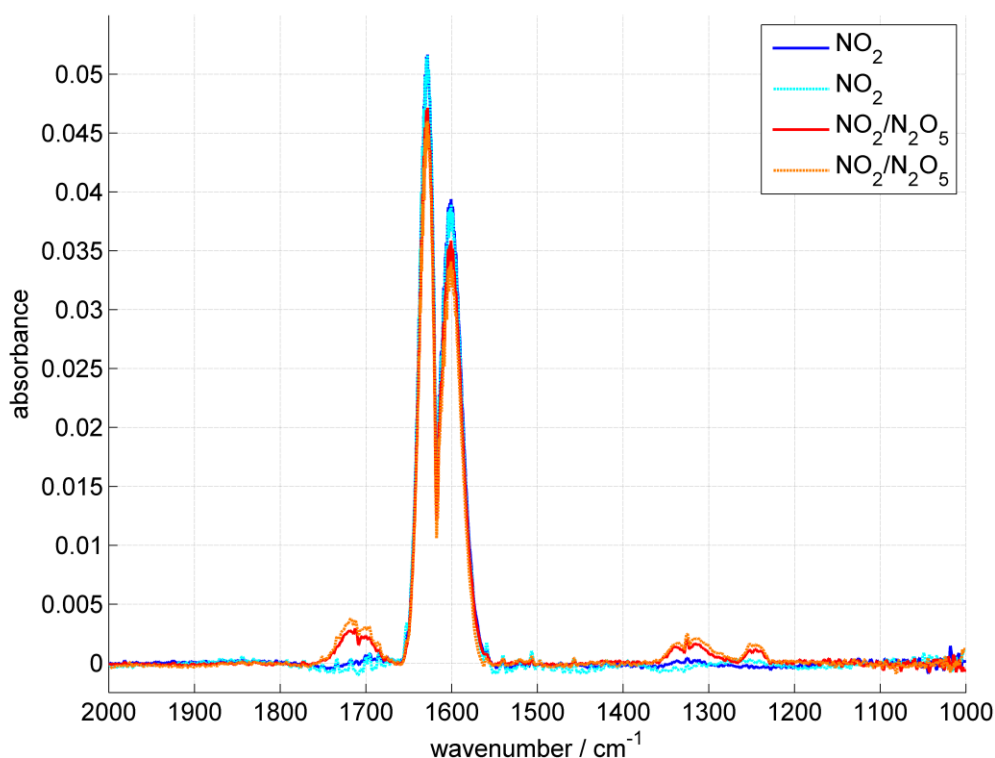


Figure 15. Absorbance spectra recorded with FTIR spectroscopy. The concentration of NO_2 was 193 ppm. The blue solid line and the light blue dashed line represents the spectra recorded for NO_2 carried by O_2 . The red solid line and the orange dashed line refer to the spectra recorded for the mixture of $\text{NO}_2 - \text{N}_2\text{O}_5$ produced by the reactions R1 – R3 and carried by O_2 . The background and baseline subtractions have been performed using the OPUS software.

The absorbance intensity increases linearly with concentration for both peaks and ϵ_{NO_2} can be calculated from the red data set. The values obtained from the linear fit to those data are: $\epsilon_{\text{NO}_2}(1600 \text{ cm}^{-1}) = (4.22 \pm 0.04) \times 10^{-19} \text{ cm}^2 \text{ molecule}^{-1}$ for the peak near 1600 cm^{-1} and $\epsilon_{\text{NO}_2}(1628 \text{ cm}^{-1}) = (5.57 \pm 0.05) \times 10^{-19} \text{ cm}^2 \text{ molecule}^{-1}$ for the peak near 1628 cm^{-1} .

The concentration of NO_2 after the reaction with ozone has been calculated using the two absorption cross sections, $\epsilon_{\text{NO}_2}(1600 \text{ cm}^{-1})$ and $\epsilon_{\text{NO}_2}(1628 \text{ cm}^{-1})$. The loss of NO_2 is almost constant as a function of the initial concentration. The NO_2 loss measured is about four times the initial O_3 concentration, hence it is double of the value expected from the model ($\approx 2.1 \times 10^{14} \text{ molecule cm}^{-3}$). In the model the equilibrium between NO_2 and N_2O_4 was not considered, and hence this may account for the extra loss of NO_2 recorded.

Furthermore, other minor reactions were not taken into account in the model, such as the NO_2 photolysis and the heterogeneous reaction on NO_2 with liquid water.¹⁰

Even if other reactions were found to affect the final concentrations of NO_2 and N_2O_5 , the amount of NO_3 produced is determined by the reactions R2 – R3, which control the

equilibrium within the $\text{NO}_2\text{-N}_2\text{O}_5\text{-NO}_3$ system, hence $[\text{NO}_3]$ can be calculated using Equation 13. The concentration of NO_3 is shown in Fig. 16 as a function of the initial $[\text{NO}_2]$. $[\text{NO}_3]$ ranges from 13 ppt to 160 ppt, which is representative for atmospheric conditions.¹¹ Any loss of NO_3 due to reactions different from the recombination with NO_2 are not taken into account for the calculation.

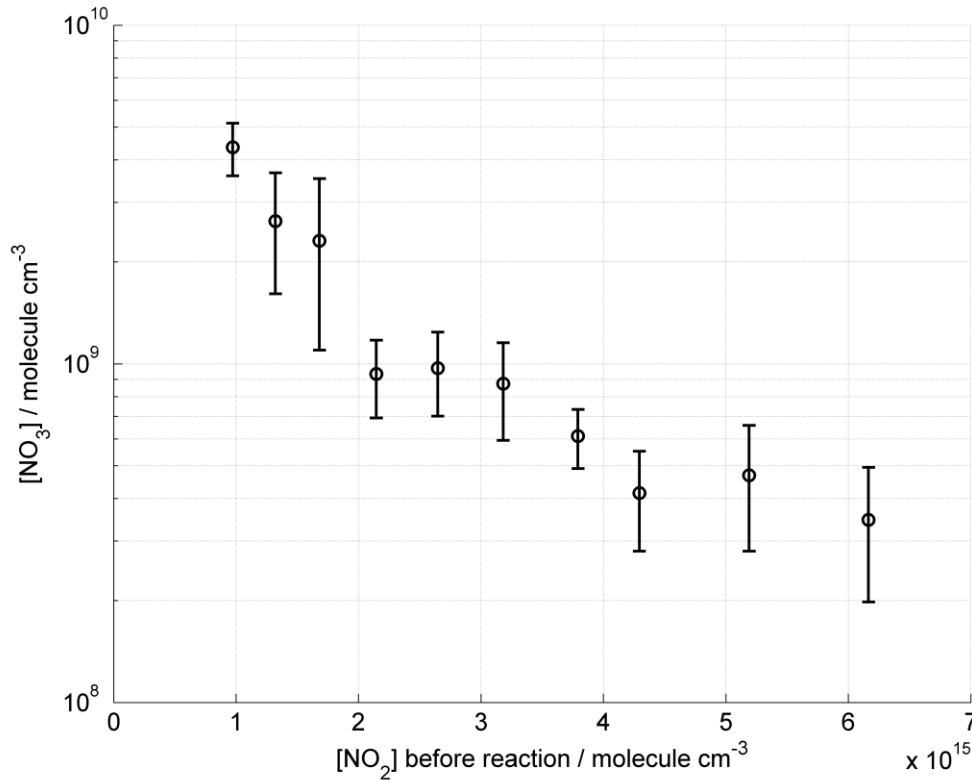


Figure 16. The concentration of NO_3 produced in reactions R1 – R3 and calculated from Eq. 12 is shown as a function of the initial concentration of NO_2 . As expected, the NO_3 production decreases as $[\text{NO}_2]$ increases.

4. Kinetic Modelling: Model Description and Fitting Procedures

4.1 Model description: gas species

In this section the description of the kinetic model is completed with all the details about the processes involving the gas species: adsorption, desorption, transport and reaction.

From the kinetic theory, the flux of colliding X_i molecules with the surface can be expressed as

$$J_{\text{coll},X_i} = \frac{\omega_{X_i}}{4} [X_i]_{gs} \quad (14)$$

where $[X_i]_{gs}$ is the near-surface gas concentration that is assumed to be the same as the gas phase concentration. As a result of the finite time required to fill the chamber, the gas-phase concentration in the chamber is described as $[X_i]_{gs} = [X_i]_v(1 - e^{-(f/v)t})$, where f is the flow

rate, v is the volume of the chamber and $[X_i]_v$ is the oxidant concentration measured by IR spectroscopy (see Section 3 for details). ω_{NO_3} is the mean thermal velocity given by $\omega_{X_i} = \sqrt{8RT/\pi M_{X_i}}$, where M_{X_i} is the molar mass of X_i , R is the gas constant and T is the absolute temperature. The flux of gas molecules adsorbed on the organic layer is expressed by

$$J_{ads,X_i} = \alpha_{s,X_i} J_{coll,X_i} \quad (15)$$

where α_{s,X_i} is the surface accommodation coefficient. In the Langmuir adsorption model, α_{s,X_i} is determined by the product of the surface accommodation coefficient on an adsorbate-free surface, $\alpha_{s,0,X_i}$, and the sorption layer coverage θ_s which is given by the sum of the surface coverage of all competing adsorbate species (*i.e.* NO_3 and NO_2).

$$\alpha_{s,X_i} = \alpha_{s,0,X_i} (1 - \sum_i \theta_{s,X_i}) = \alpha_{s,0,X_i} (1 - \sum_i \sigma_{X_i} [X_i]_s) \quad (16)$$

The surface coverage is defined as the ratio between the actual and the maximum surface concentration value of the gas species, X_i :

$$\theta_{s,X_i} = [X_i]_s / [X_i]_{s,max} = \sigma_{X_i} [X_i]_s \quad (17)$$

The adsorbed molecule can thermally desorb back to the gas phase.

Desorption can be described by a first-order rate coefficient, k_{d,X_i} , which is assumed to be independent of θ_{s,X_i} . The flux of desorption of gas-phase molecules can be expressed as

$$J_{des,X_i} = k_{d,X_i} [X_i]_s = \tau_{d,X_i}^{-1} [X_i]_s \quad (18)$$

The desorption lifetime τ_{d,X_i} is the mean residence time on the surface in the absence of surface reaction and surface bulk transport. For NO_3 we assume to have two desorption lifetimes, $\tau_{d,NO_3,1}$ and $\tau_{d,NO_3,2}$, which are combined to give an effective desorption time $\tau_{d,NO_3,eff}$ weighted by the organic surface coverage, $\theta_{ss} = [Y]_{ss} / [Y]_{ss,0}$ as

$$\tau_{d,NO_3,eff}^{-1} = \theta_{ss} \tau_{d,NO_3,1}^{-1} + (1 - \theta_{ss}) \tau_{d,NO_3,2}^{-1} \quad (19)$$

This change in desorption time is related to the change of orientation of the organic molecules at the interface, *i.e.* for a highly packed monolayer the reactive site is assumed to be less accessible, and the oxidant has less affinity for other parts of the molecules hence the desorption is faster. When the organic surface coverage decreases the reactive sites become more accessible and the desorption is slowed down. For NO_2 we considered a single

desorption lifetime, τ_{d,NO_2} . Once adsorbed to the surface, the gas-phase molecules can be transported to the bulk water and vice versa. The corresponding fluxes can be expressed as

$$J_{sb, X_i} = k_{sb, X_i} [X_i]_s \quad (20)$$

$$J_{bs, X_i} = k_{bs, X_i} [X_i]_b \quad (21)$$

where k_{bs, X_i} in cm s^{-1} is a transport coefficient and can be regarded as effective transport velocity. The bulk diffusion coefficient, D_{b, X_i} , can be used to estimate this transport velocity, $k_{bs, X_i} \approx 4D_{b, X_i} / \pi \lambda_{X_i}$ where λ_{X_i} is the average travel distance from the near-surface bulk into the sorption layer. To estimate k_{sb, X_i} the rate coefficients for gas–surface and surface–bulk transport can be matched with a literature value or estimate for the Henry's law coefficient or gas–particle equilibrium partitioning coefficient (H_{X_i}):

$$k_{sb, X_i} = \frac{4k_{bs, X_i} H_{X_i}}{\alpha_{s, X_i} \tau_{d, X_i} \omega_{X_i}} \quad (22)$$

4.2 Fitting Results

4.2.1 dOA exposed to NO_3

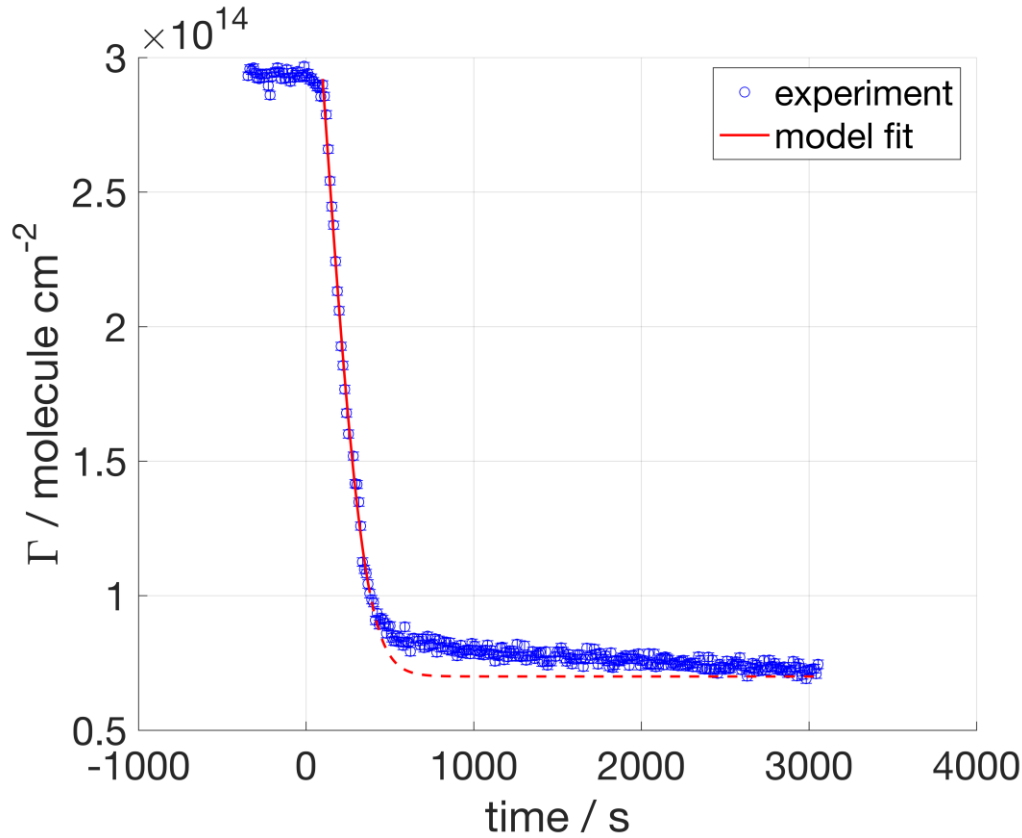


Figure 17. dOA exposed to 86 ppt NO_3 .

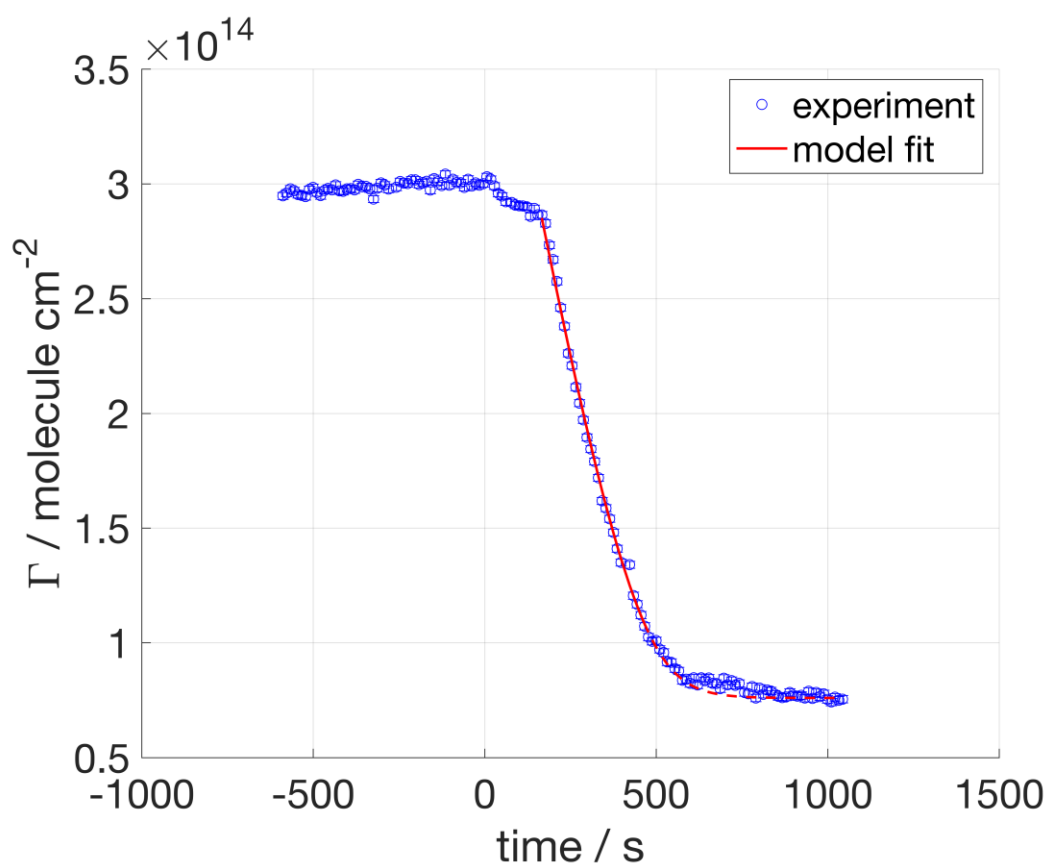


Figure 18. dOA exposed to 86 ppt NO_3 .

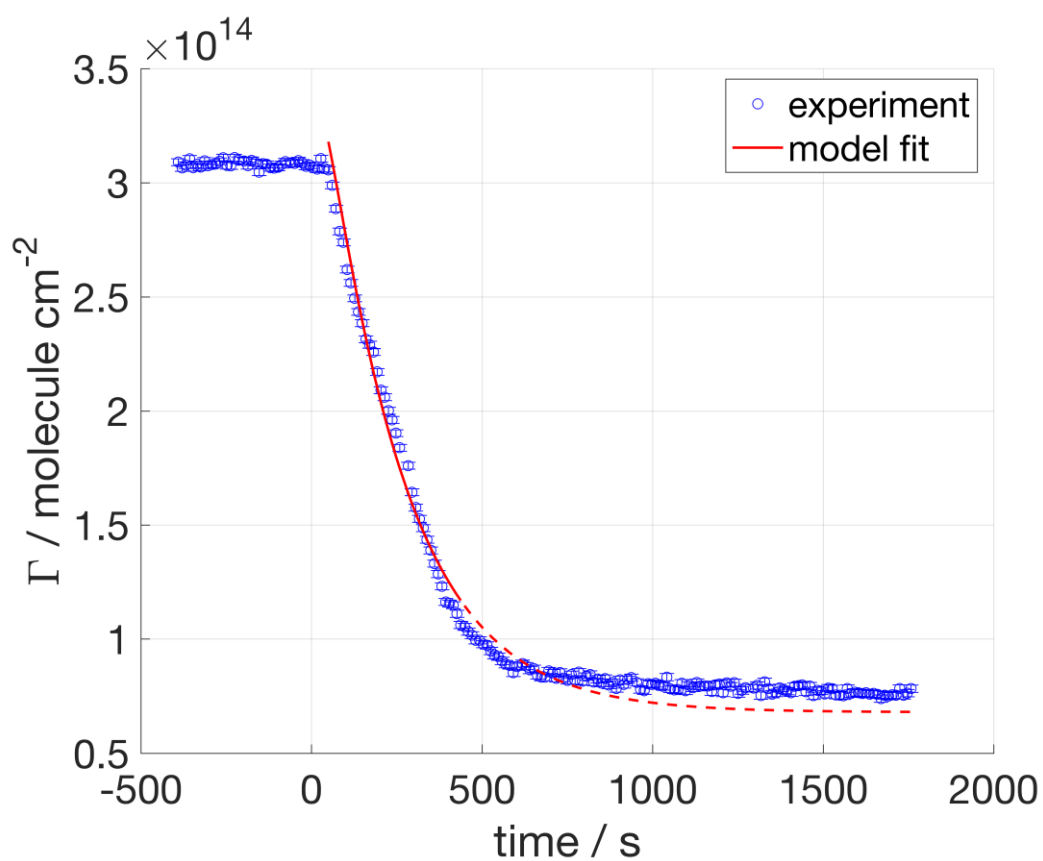


Figure 19. dOA exposed to 35 ppt NO_3 .

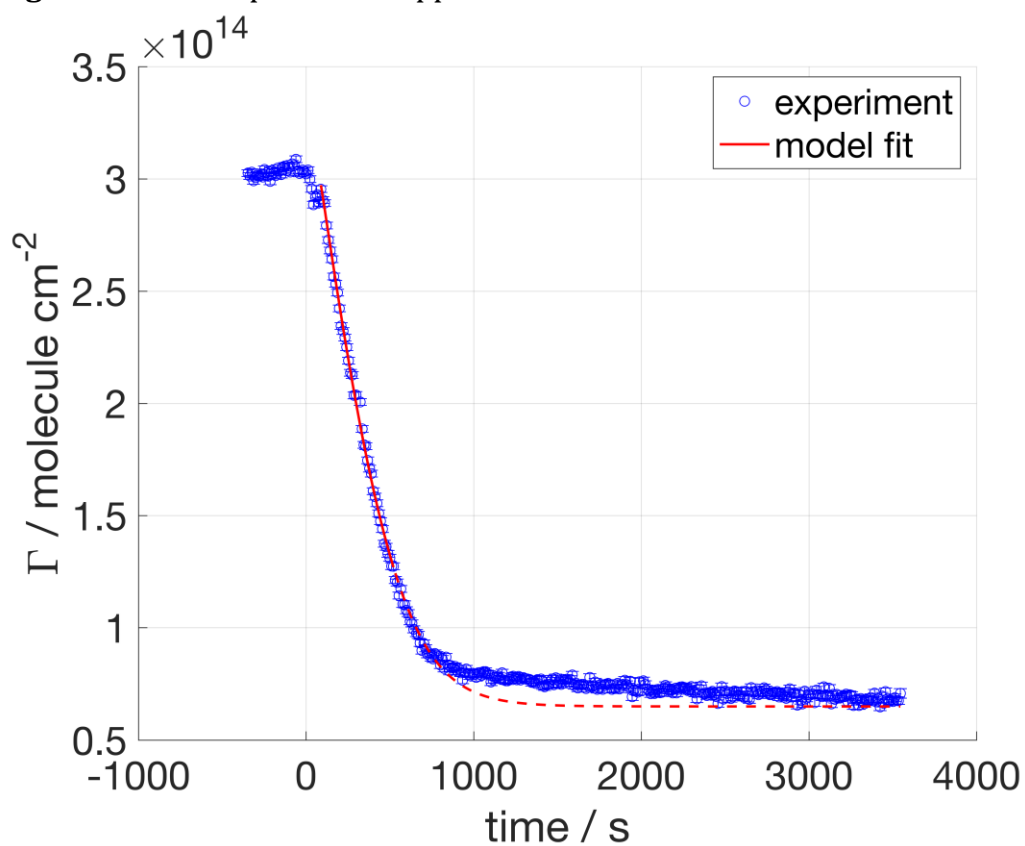


Figure 20. dOA exposed to 36 ppt NO_3 .

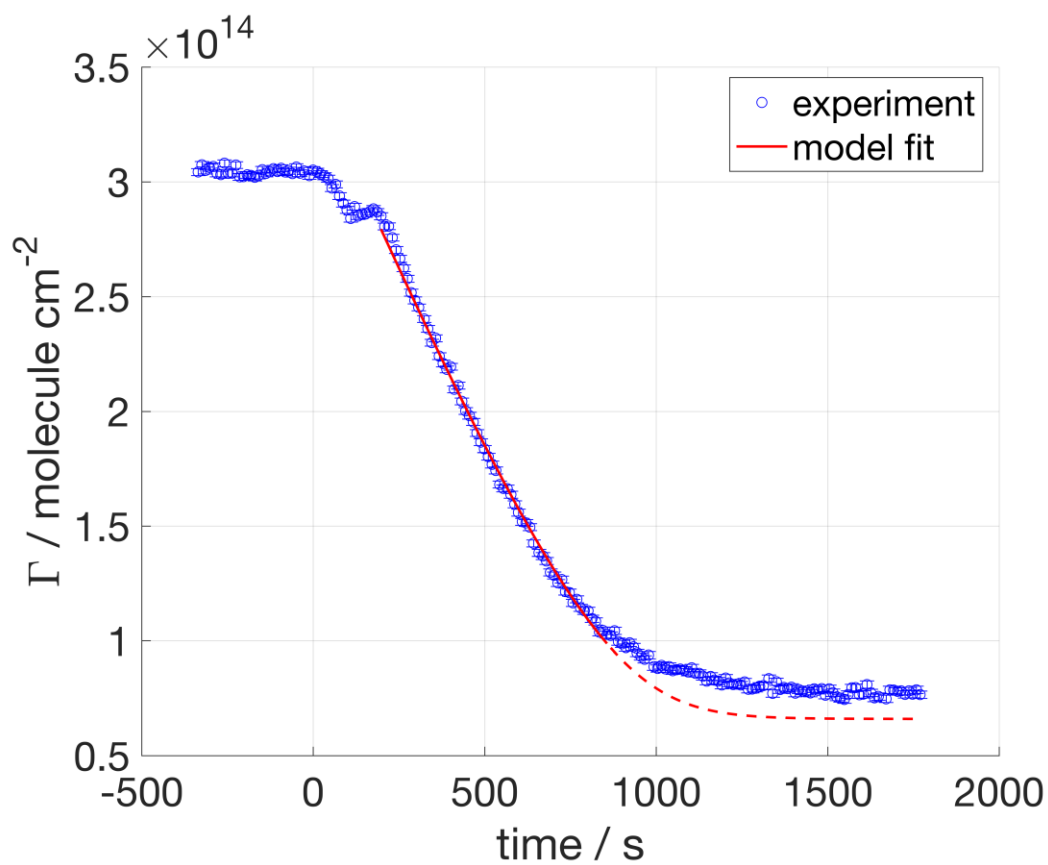


Figure 21. dOA exposed to 36 ppt NO_3 .

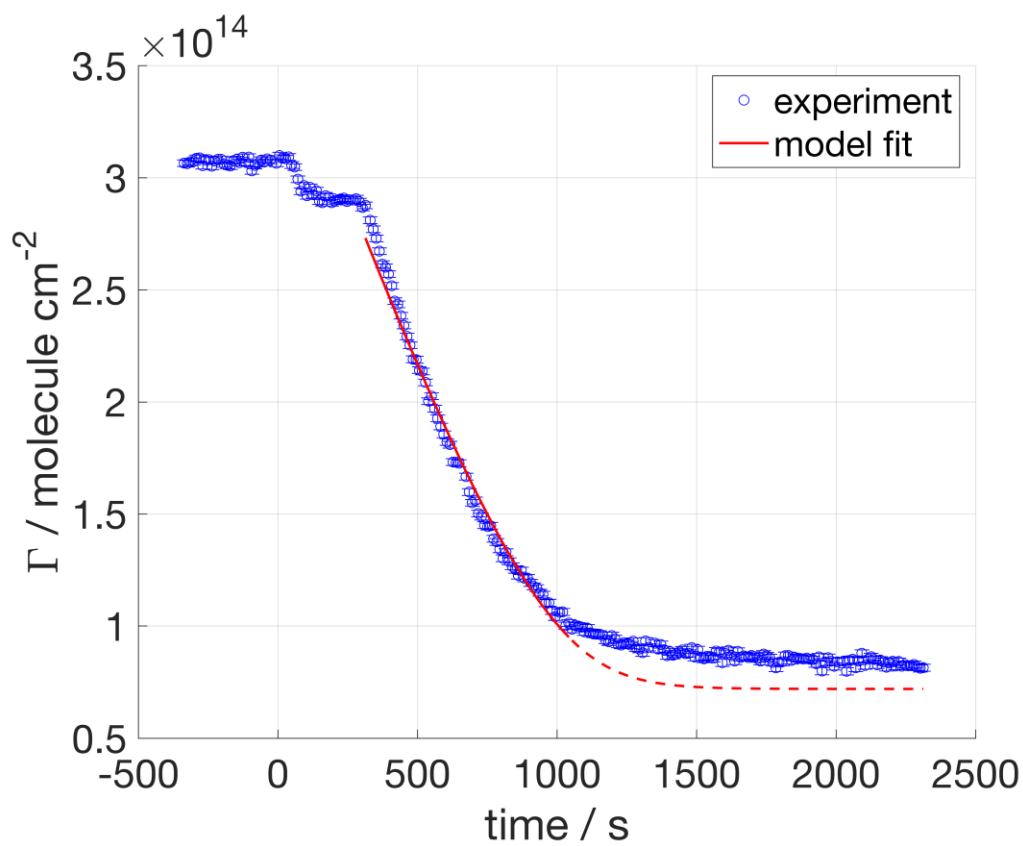


Figure 22. dOA exposed to 32 ppt NO_3 .

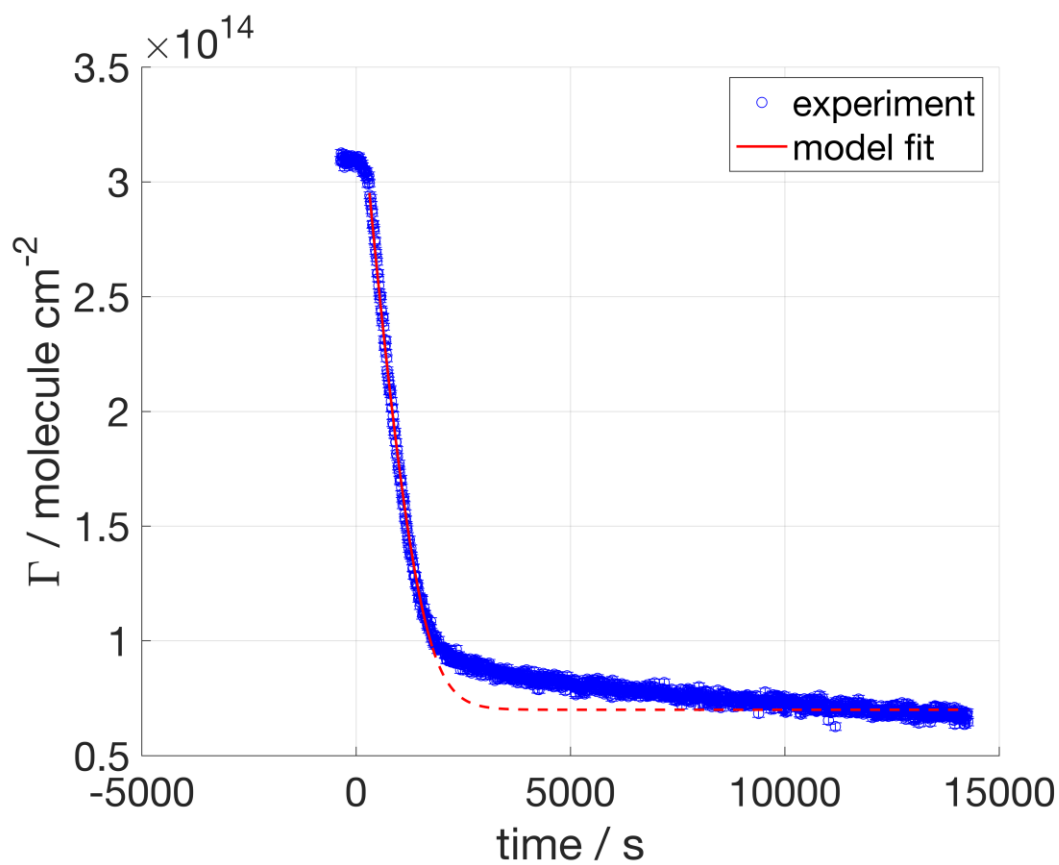


Figure 23. dOA exposed to 15 ppt NO_3 .

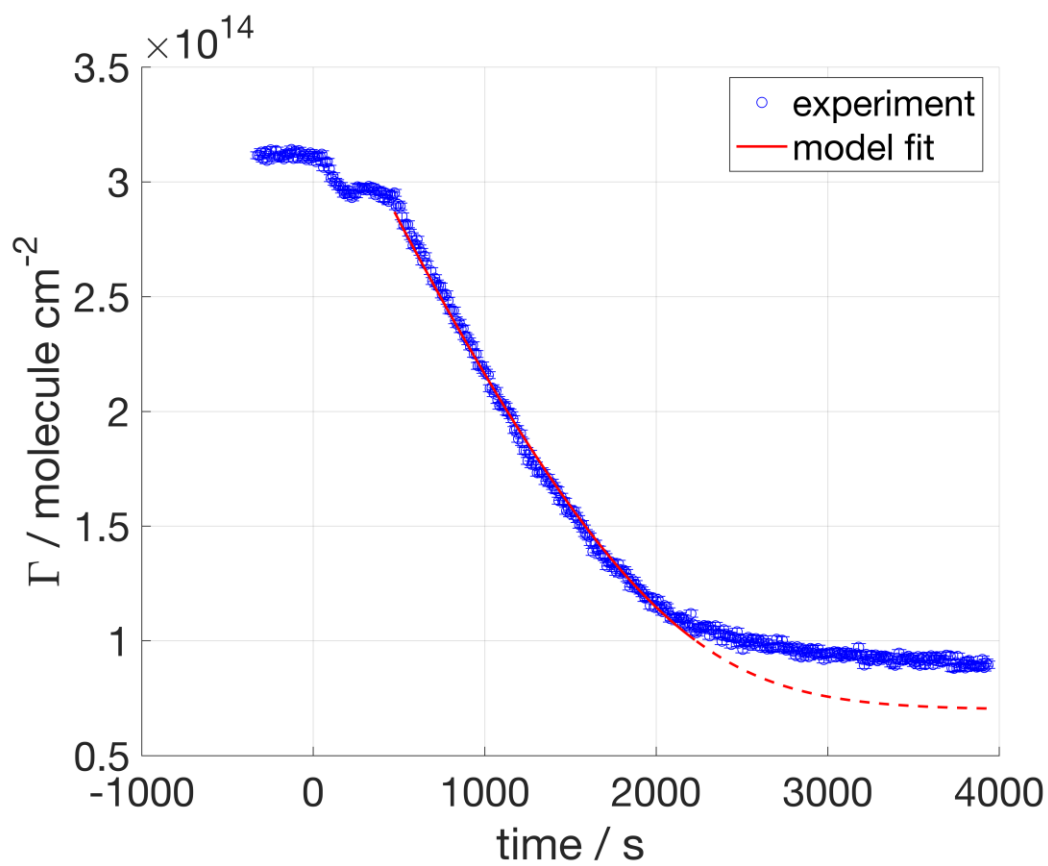


Figure 24. dOA exposed to 15 ppt NO_3 .

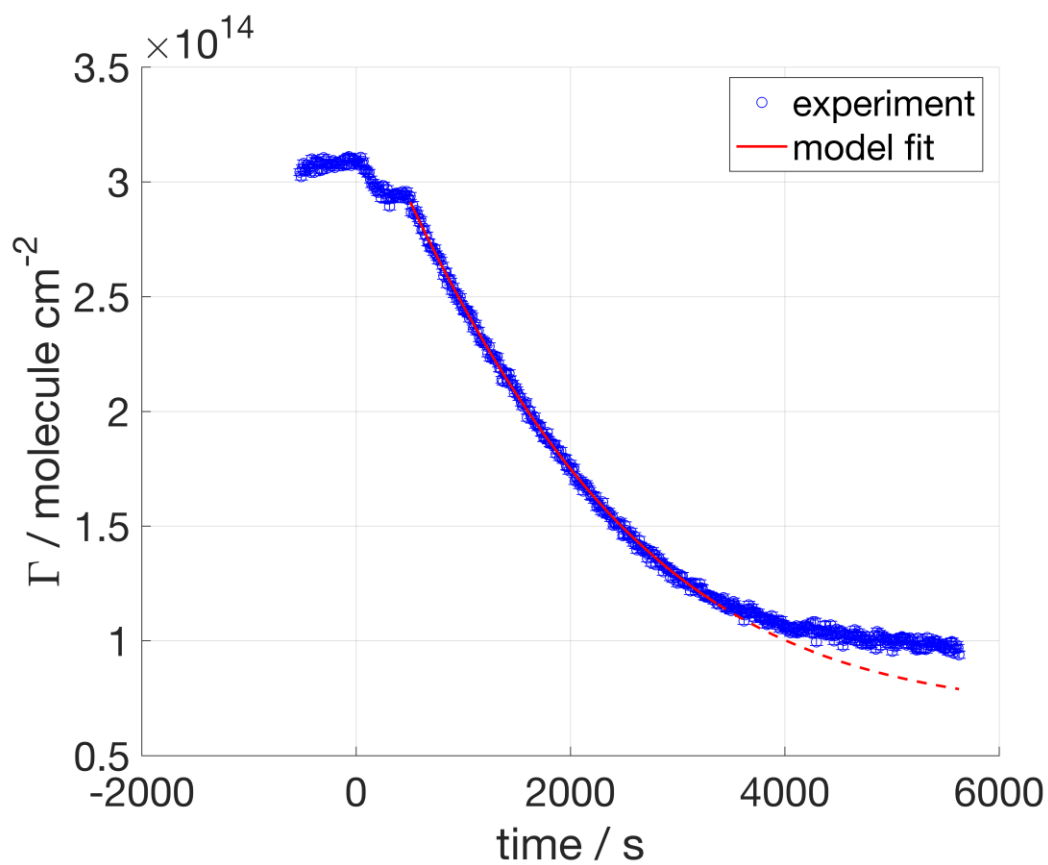


Figure 25. dOA exposed to 13 ppt NO_3 .

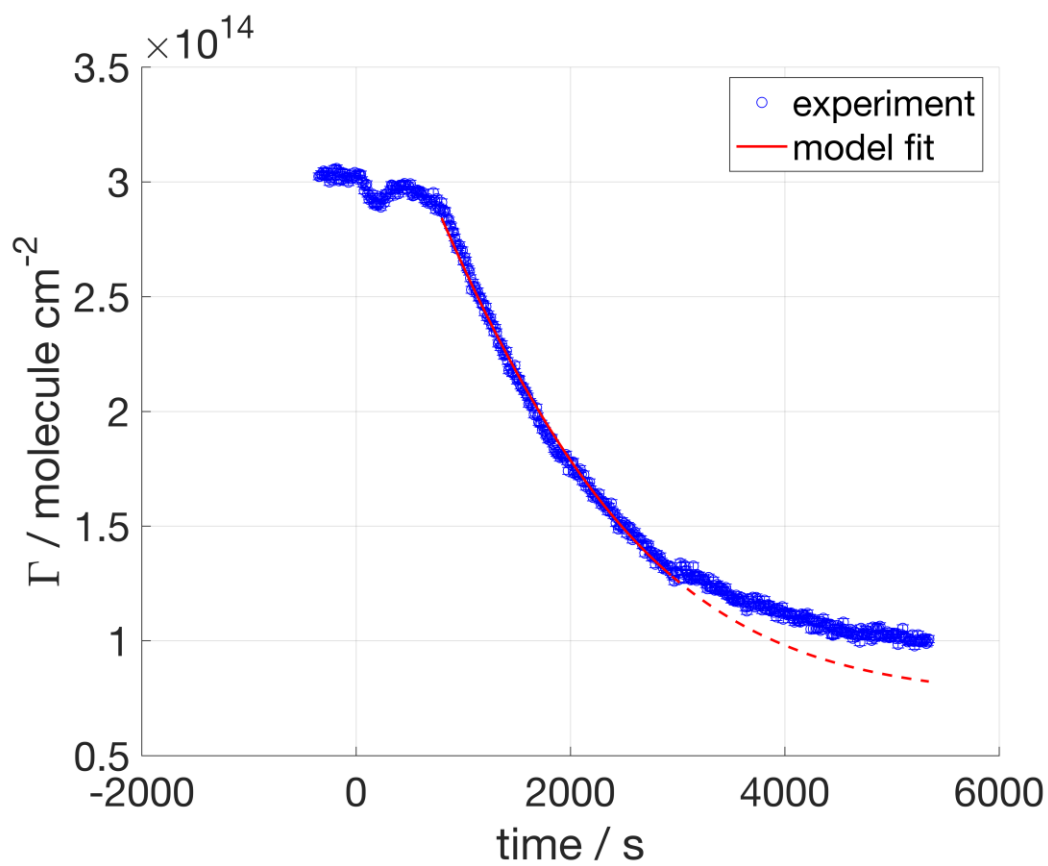
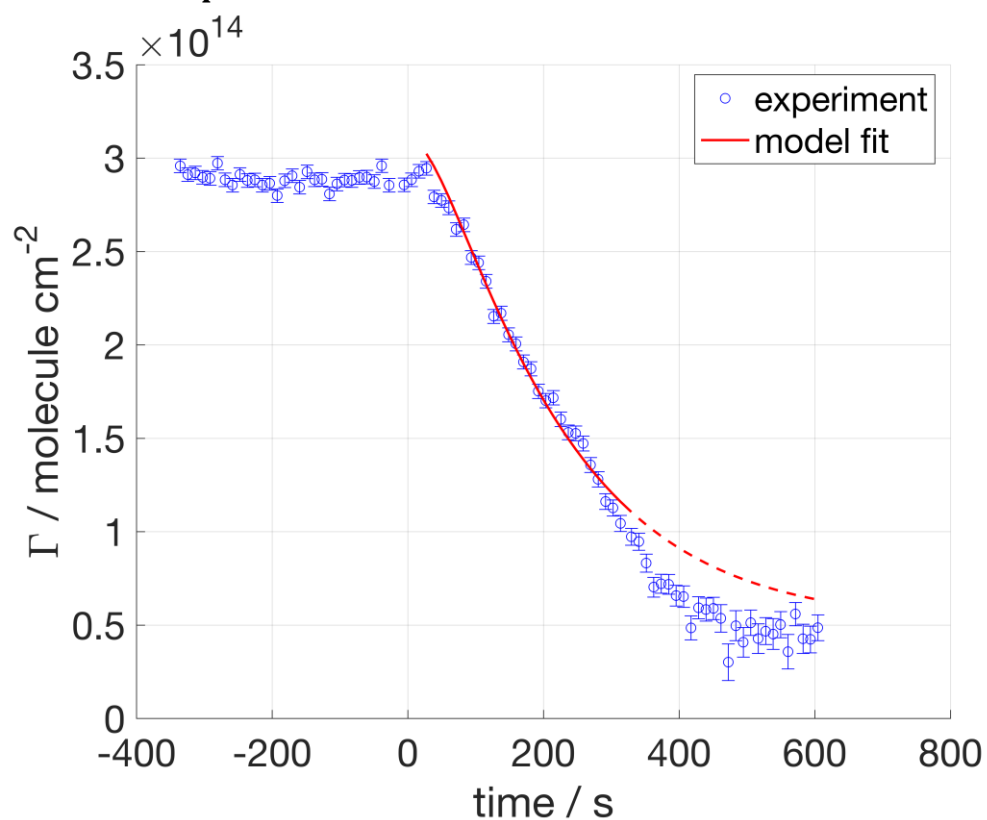
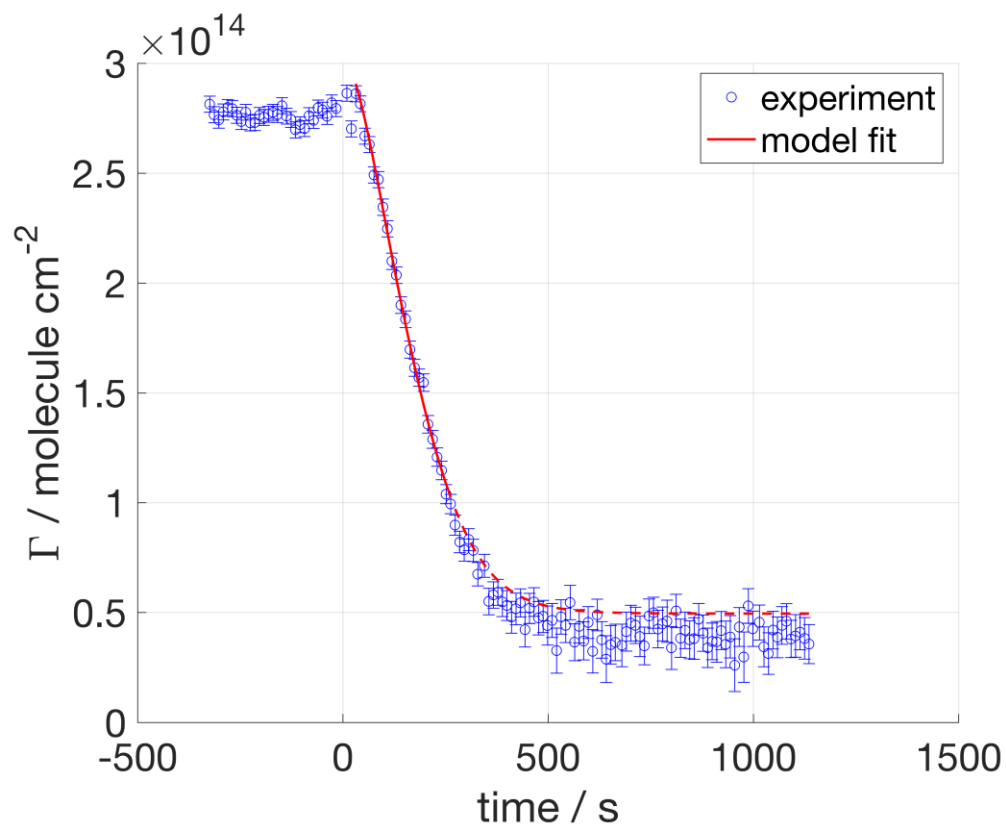


Figure 26. dOA exposed to 13 ppt NO_3 .

1
2 **4.2.2 dPOA exposed to NO₃**

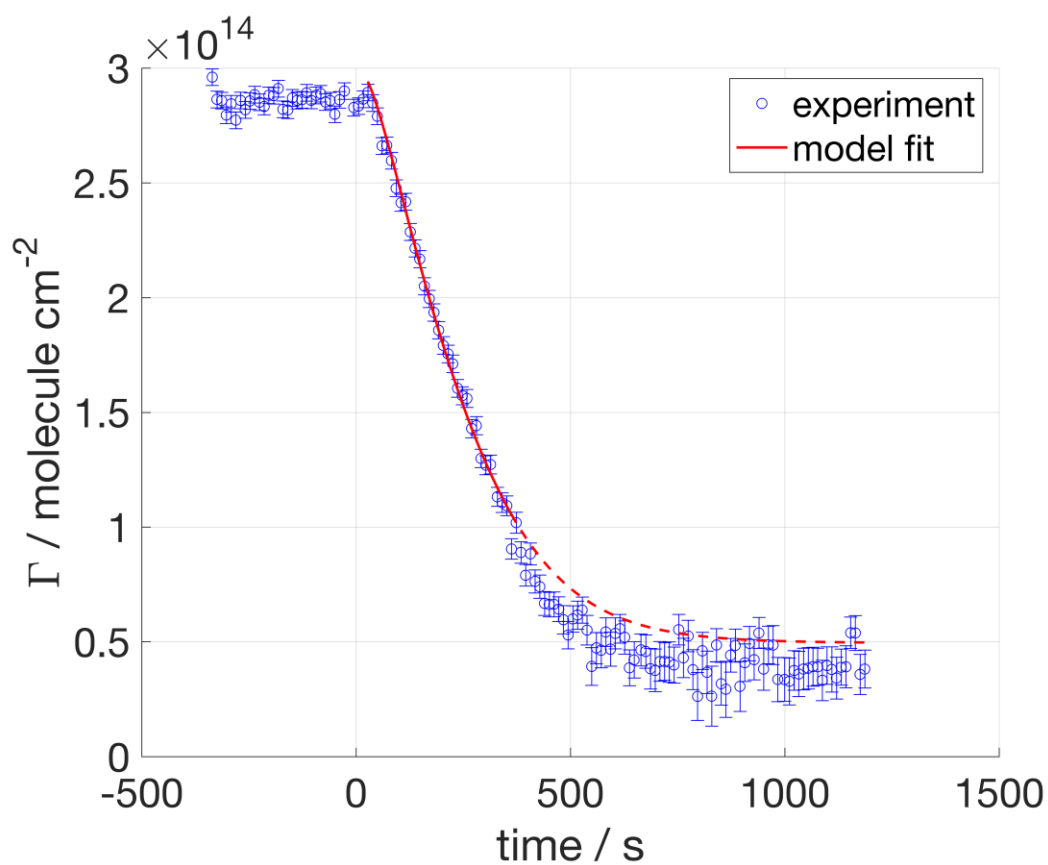


3
4 **Figure 27.** dPOA exposed to 86 ppt NO₃.
5

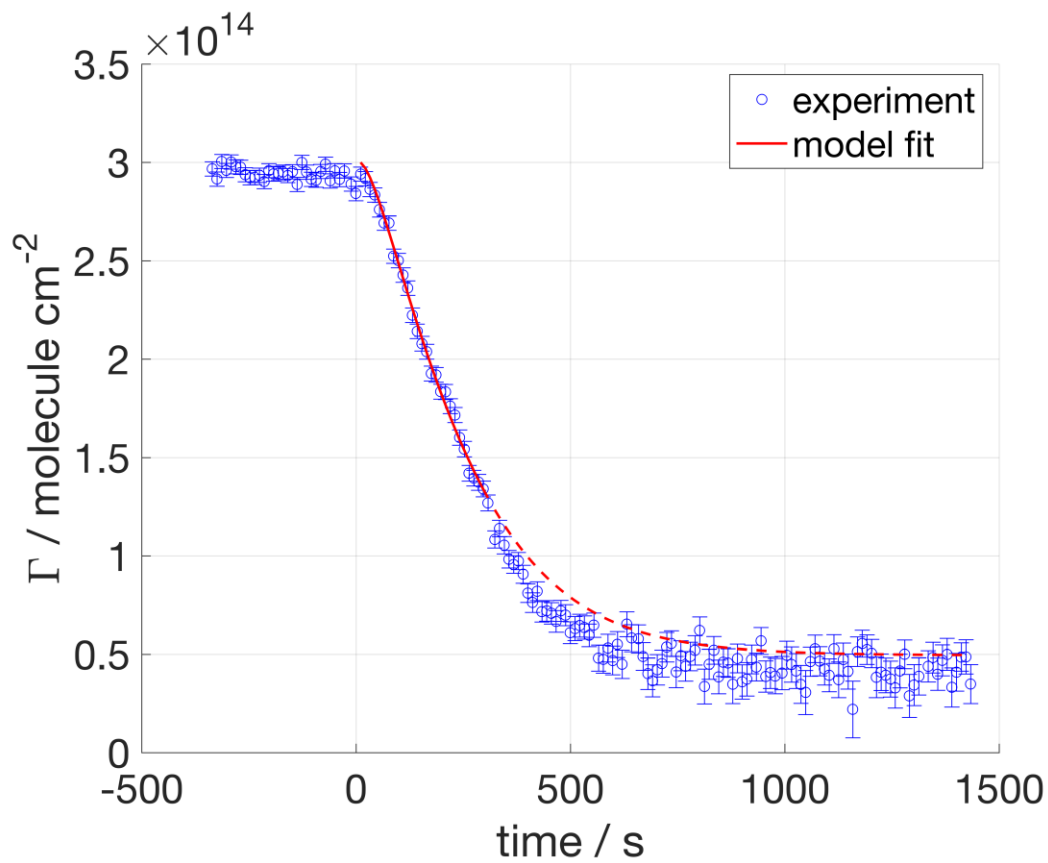


6
7 **Figure 28.** dPOA exposed to 86 ppt NO₃.

1



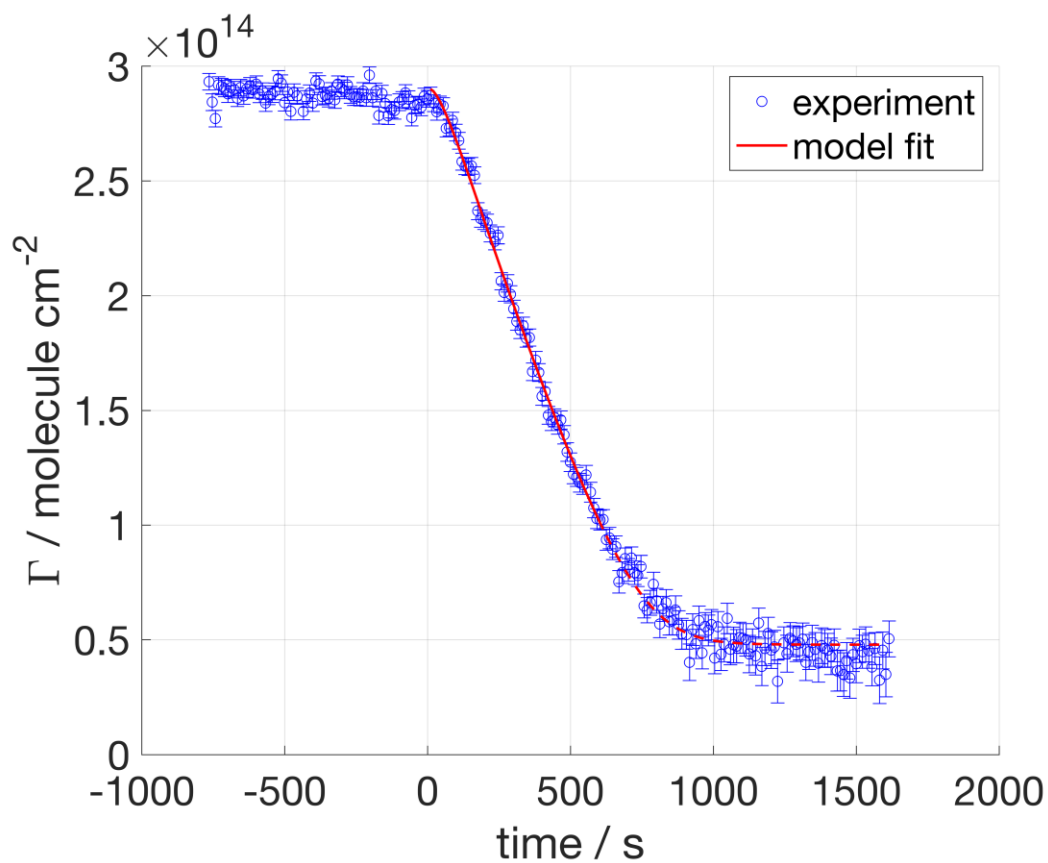
2

3 **Figure 29.** dPOA exposed to 35 ppt NO_3 .

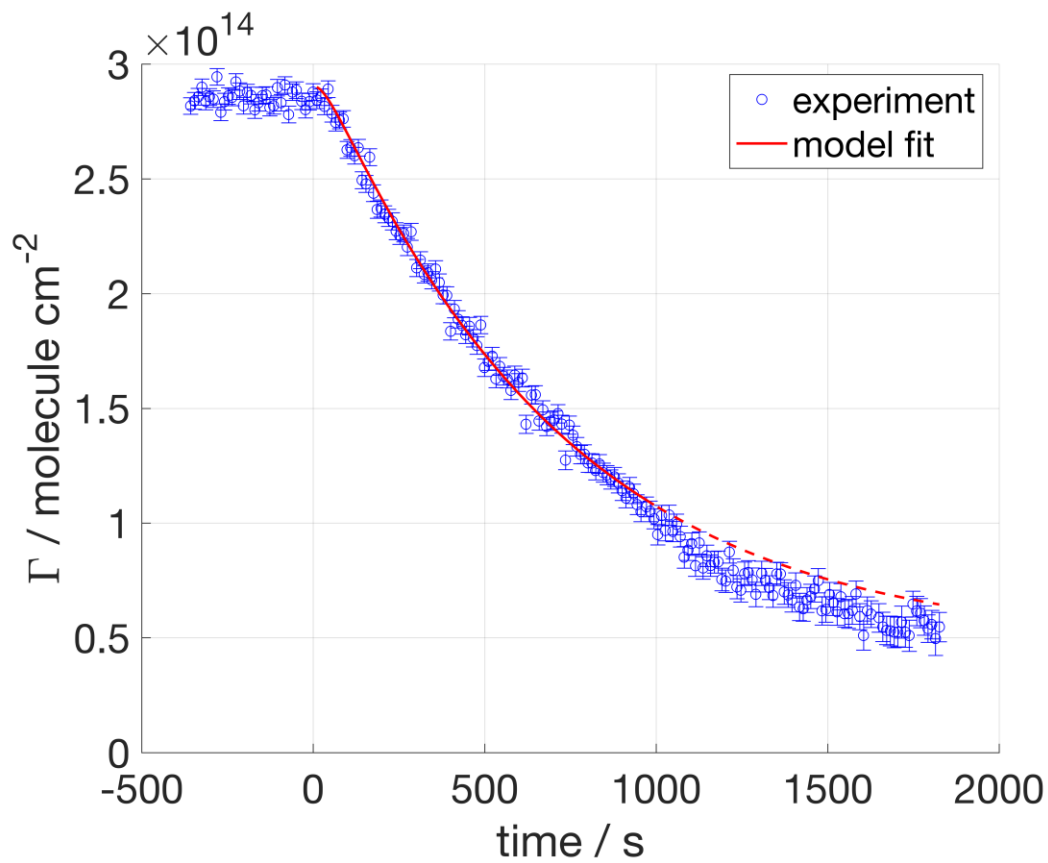
4

5 **Figure 30.** dPOA exposed to 36 ppt NO_3 .

1



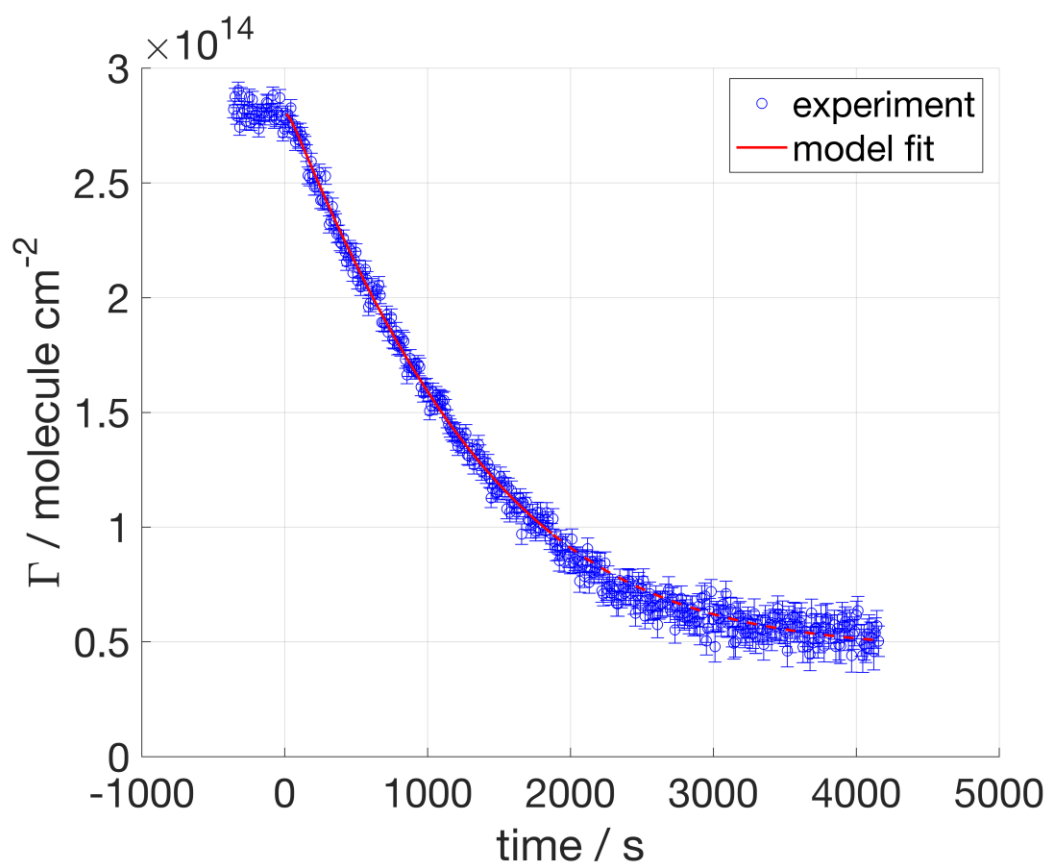
2

3 **Figure 31.** dPOA exposed to 32 ppt NO_3 .

4

5 **Figure 32.** dPOA exposed to 15 ppt NO_3 .

1



2

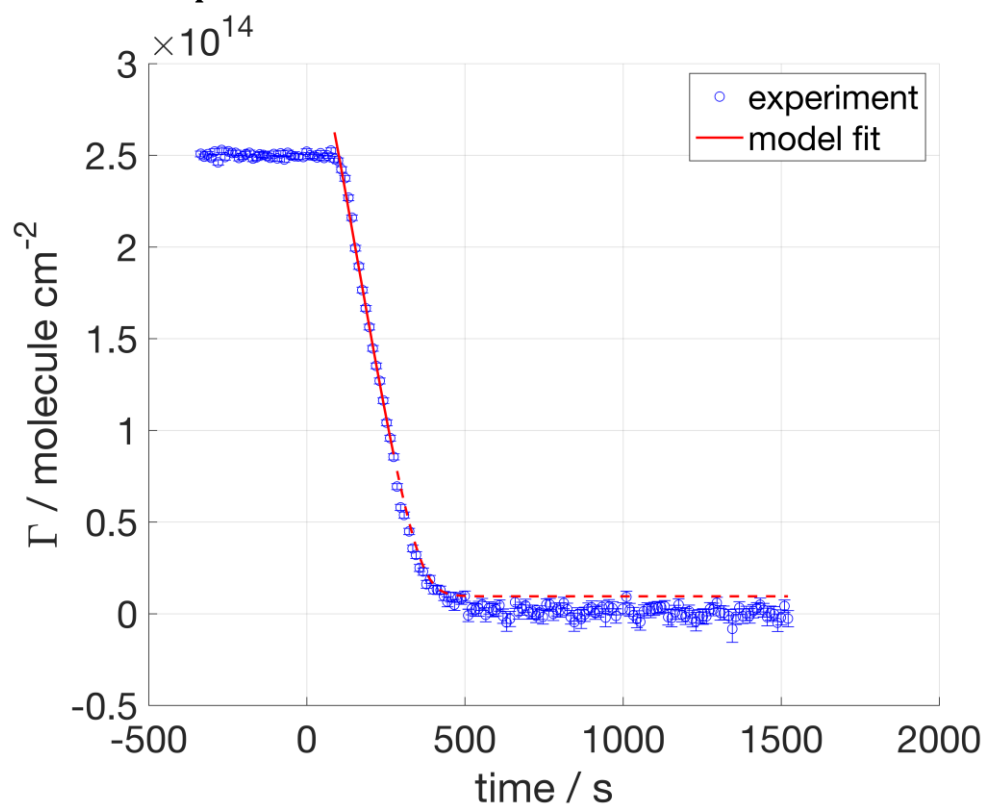
Figure 33. dPOA exposed to 13 ppt NO_3 .

3

4

5

4.2.3 dMO exposed to NO_3

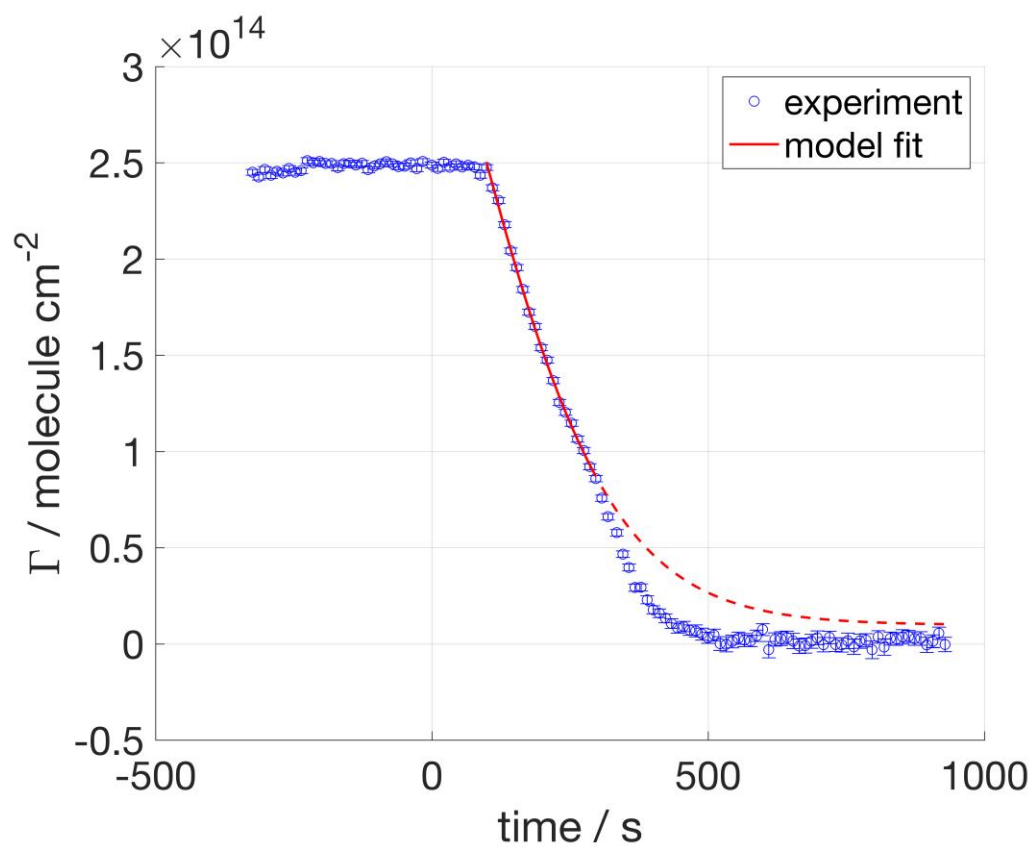


6

7

Figure 34. dMO exposed to 86 ppt NO_3 .

1

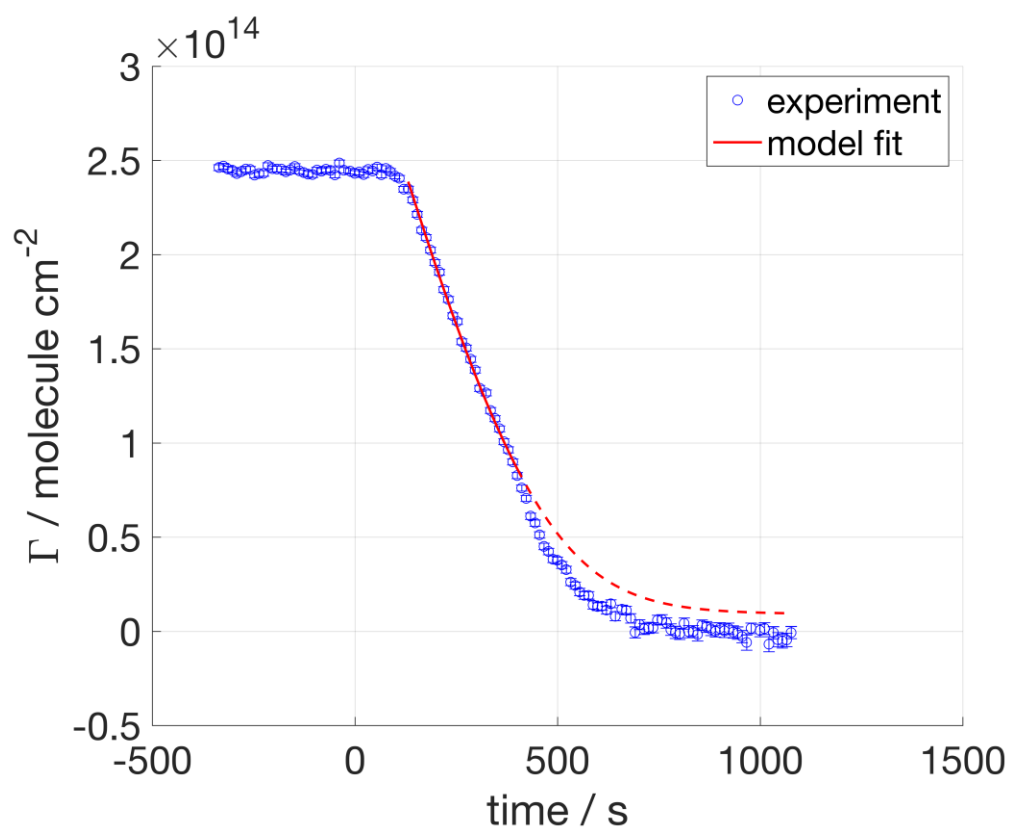


2

3

Figure 35. dMO exposed to 86 ppt NO_3 .

4



5

6

Figure 36. dMO exposed to 36 ppt NO_3 .

7

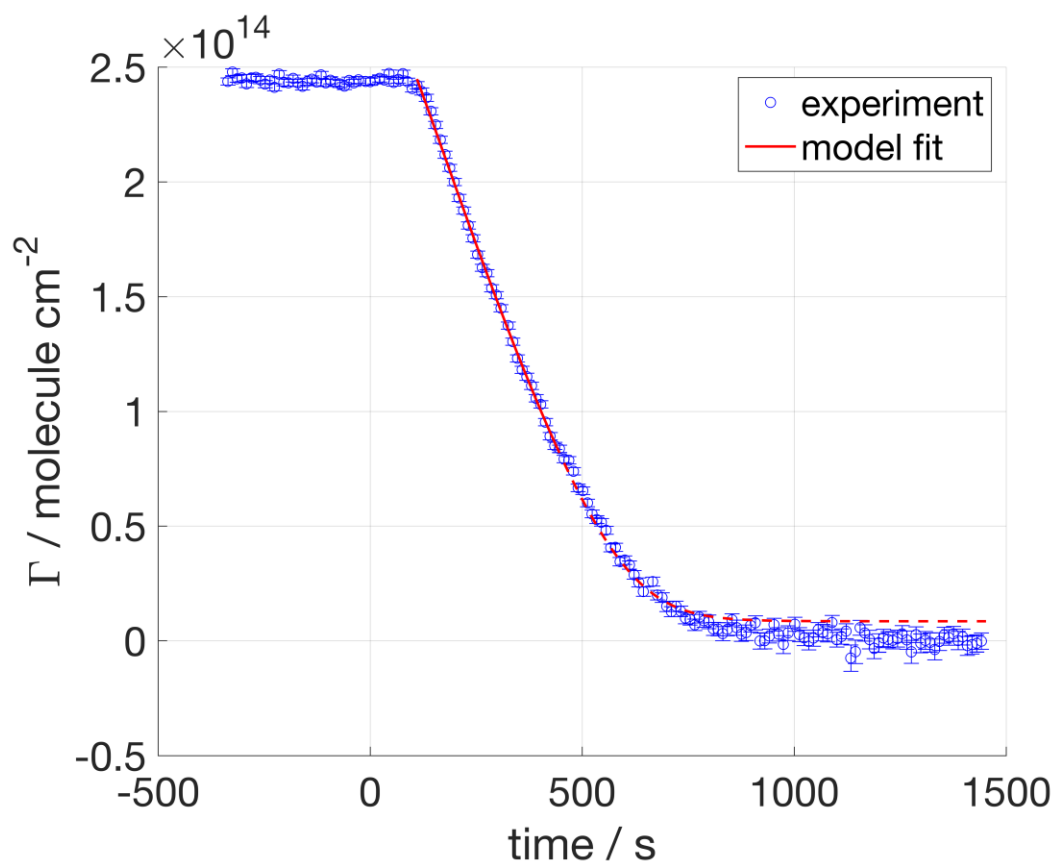


Figure 37. dMO exposed to 36 ppt NO_3 .

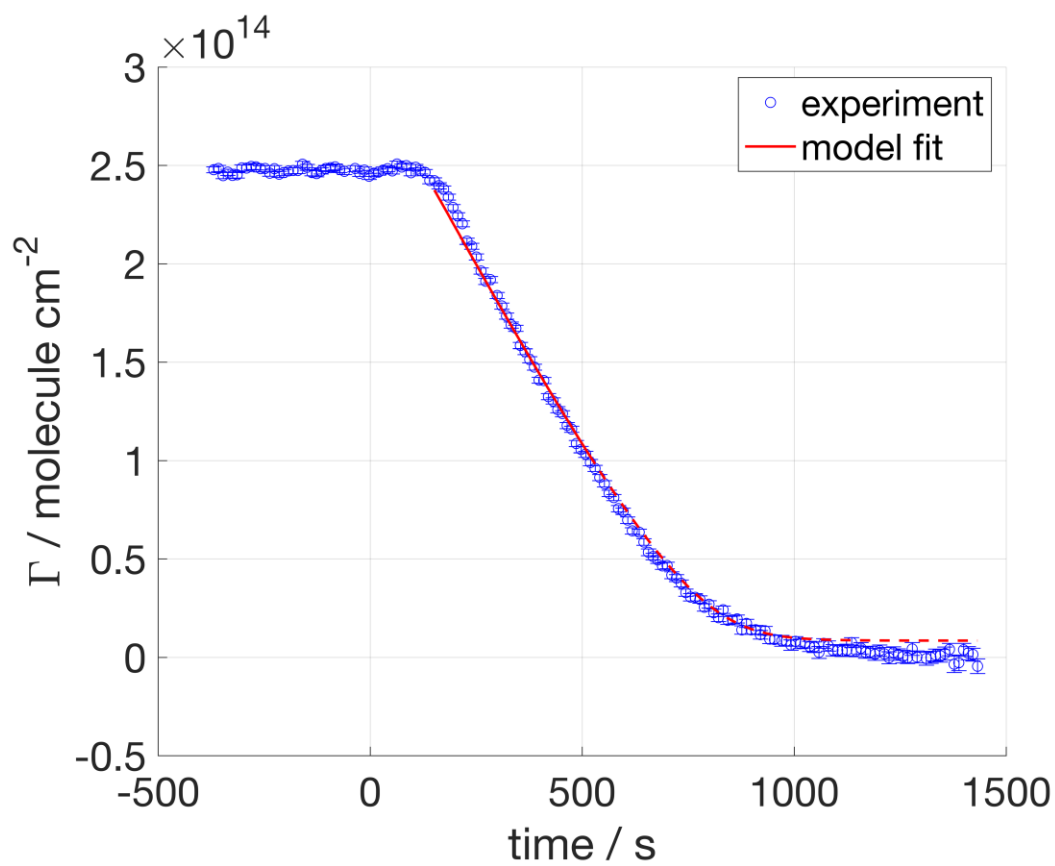


Figure 38. dMO exposed to 32 ppt NO_3 .

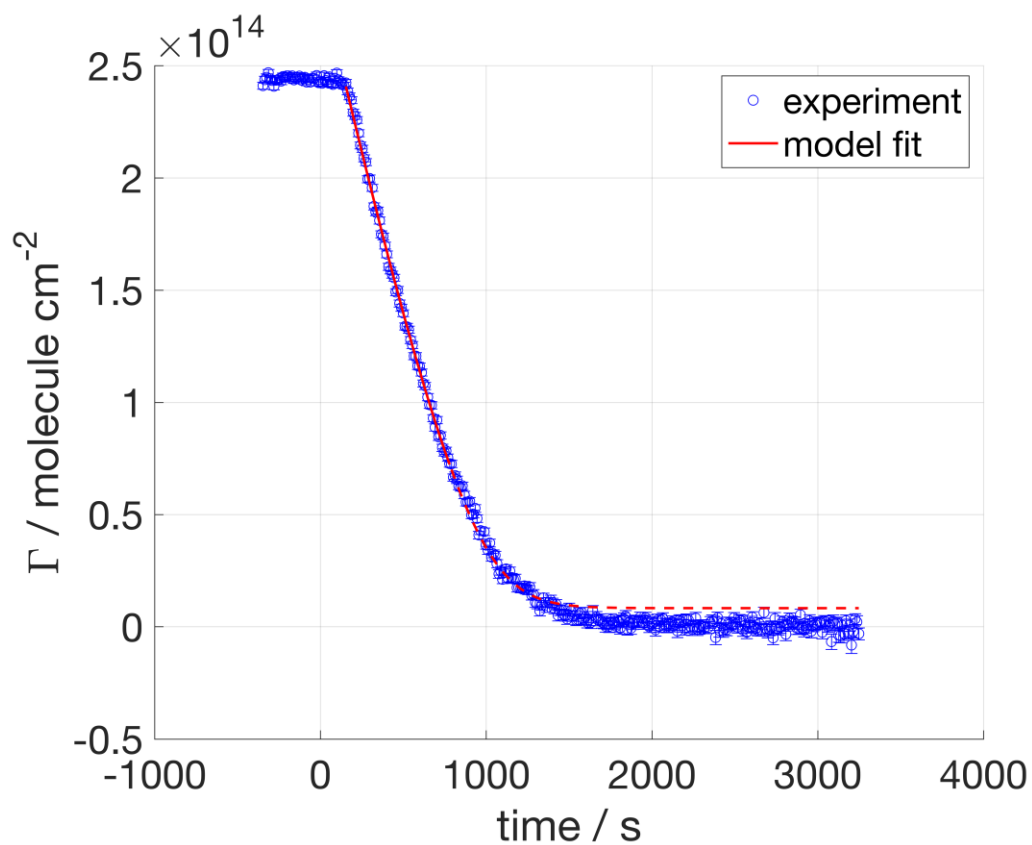


Figure 39. dMO exposed to 15 ppt NO_3 .

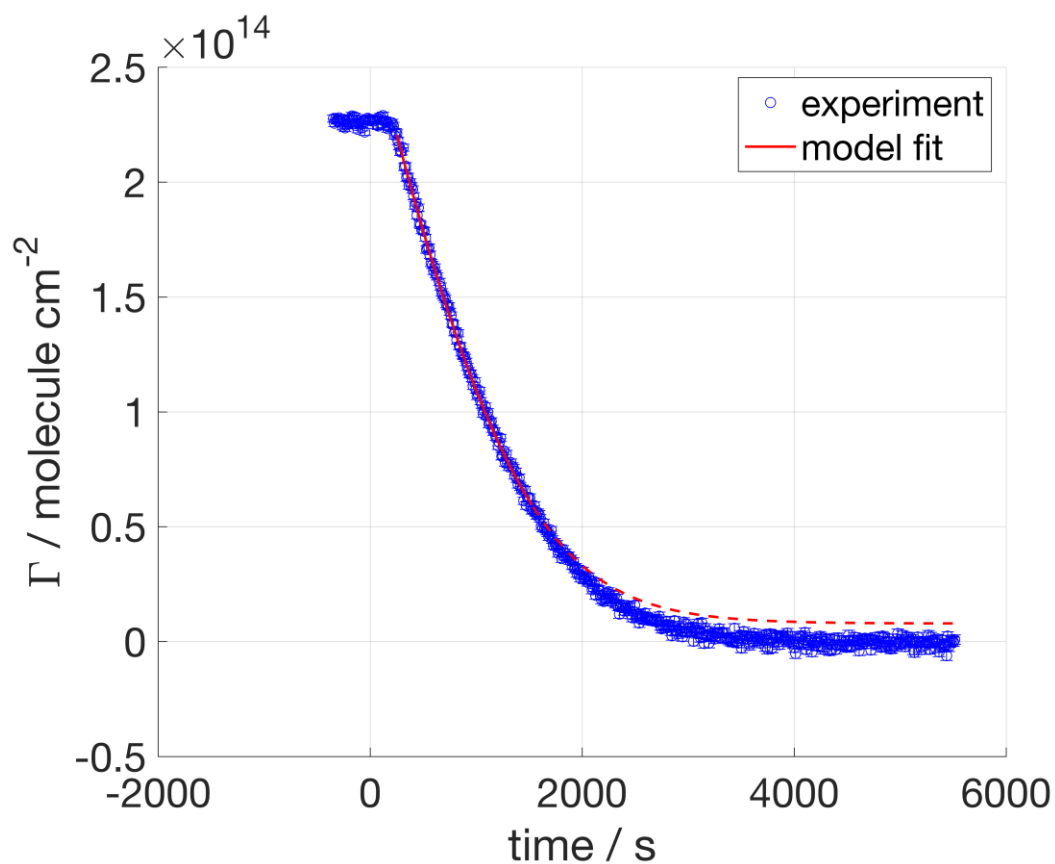


Figure 40. dMO exposed to 13 ppt NO_3 .

4.2.4 dSA exposed to NO₃

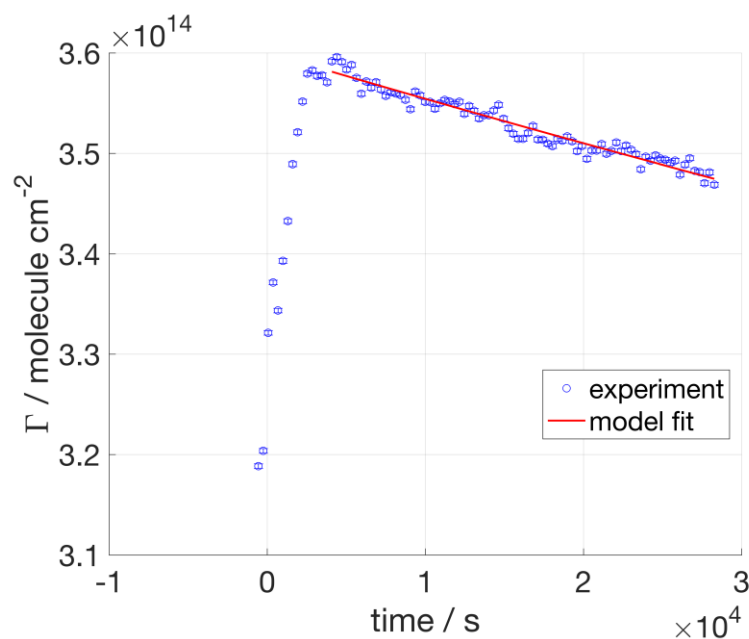


Figure 41. Stearic acid (*d*₃₅SA) exposed to [NO₃] = 86 ppt. The red line illustrates the fit obtained from our kinetic modelling.

References

1. Barnes, G. & Gentle, I. *Interfacial science: an introduction*. (Oxford University Press, 2010).
2. Sander, S. P. *et al.* Chemical Kinetics and Photochemical Data for Use in Atmospheric Studies, Evaluation No. 17. *JPL Publ.* 10-6 (2011).
3. Seinfeld, J. H. & Pandis, S. N. *Atmospheric Chemistry and Physics: From Air Pollution to Climate Change*. (John Wiley & Sons, Inc., 2006).
4. Troe, J. Specific rate constant *k*(*E*,*J*) for unimolecular bond fission. *J. Chem. Phys.* **79**, 6017–6029 (1983).
5. MATLAB. *version 7.12.0 (R2011a)*. (The Math Works Inc., 2011).
6. Guttman, A. Absolute infrared intensity measurements on nitrogen dioxide and dinitrogen tetroxide. *J. Quant. Spectrosc. Radiat. Transf.* **2**, 1–15 (1961).
7. Cantrell, C. A., Davidson, J. A., McDaniel, A. H., Shetter, R. E. & Calvert, J. G. Infrared absorption cross sections for N₂O₅. *Chem. Phys. Lett.* **148**, 358–363 (1988).
8. Hjorth, J., Ottobriani, G., Cappellani, F. & Restelli, G. A Fourier transform infrared study of the rate constant of the homogeneous gas-phase reaction nitrogen oxide (N₂O₅) + water and determination of absolute infrared band intensities of N₂O₅ and nitric acid. *J. Phys. Chem.* **91**, 1565–1568 (1987).
9. Chackerian, C., Sharpe, S. W. & Blake, T. A. Anhydrous nitric acid integrated absorption cross sections: 820–5300 cm⁻¹. *J. Quant. Spectrosc. Radiat. Transf.* **82**, 429–441 (2003).

- 1 10. Ammann, M. *et al.* Evaluated kinetic and photochemical data for atmospheric
2 chemistry: Volume VI - heterogeneous reactions with liquid substrates. *Atmos.*
3 *Chem. Phys.* **13**, 8045–8228 (2013).
- 4 11. Brown, S. S. & Stutz, J. Nighttime radical observations and chemistry. *Chem. Soc.*
5 *Rev.* **41**, 6405–6447 (2012).
- 6 12. King, M. D., Rennie, A. R., Pfrang, C., Hughes, A. V & Thompson, K. C. Interaction of
7 nitrogen dioxide (NO₂) with a monolayer of oleic acid at the air–water interface –
8 A simple proxy for atmospheric aerosol. *Atmos. Environ.* **44**, 1822–1825 (2010).
9